Journal Pre-proof

Selective extraction of platinum and palladium using reusable carvacrol-based deep eutectic solvents: experimental and computational insights

Sahar Gholami, Pablo López-Porfiri, María Pérez-Page, Jesús Esteban

PII: S1383-5866(26)00858-0

DOI: https://doi.org/10.1016/j.seppur.2026.137592

Reference: SEPPUR 137592

To appear in:

Received date: 25 December 2025

Revised date: 28 February 2026

Accepted date: 12 March 2026

Please cite this article as: S. Gholami, P. López-Porfiri, M. Pérez-Page, et al., Selective extraction of platinum and palladium using reusable carvacrol-based deep eutectic solvents: experimental and computational insights, (2024), https://doi.org/10.1016/j.seppur.2026.137592

This is a PDF of an article that has undergone enhancements after acceptance, such as the addition of a cover page and metadata, and formatting for readability. This version will undergo additional copyediting, typesetting and review before it is published in its final form. As such, this version is no longer the Accepted Manuscript, but it is not yet the definitive Version of Record; we are providing this early version to give early visibility of the article. Please note that Elsevier's sharing policy for the Published Journal Article applies to this version, see: https://www.elsevier.com/about/policies-and-standards/sharing#4-published-journal-article. Please also note that, during the production process, errors may be discovered which could affect the content, and all legal disclaimers that apply to the journal pertain.

© 2026 Published by Elsevier B.V.

Journal Pre-proof

Selective Extraction of Platinum and Palladium Using Reusable Carvacrol-Based Deep Eutectic Solvents: Experimental and Computational Insights

Sahar Gholami[a], Pablo López-Porfiri[a], María Pérez-Page[a*], Jesús Esteban[b,a *]

[a] *Department of Chemical Engineering, School of Engineering, The University of Manchester. Oxford Road. Manchester, M13 9PL, United Kingdom.*
[b] *Department of Chemical Engineering and Materials, Faculty of Chemical Sciences, Complutense University of Madrid. Avda. Complutense s/n, 28040 Madrid, Spain*

First author: sahar.gholami@manchester.ac.uk

Corresponding author: jeesteba@ucm.es; jesus.estebanserrano@manchester.ac.uk; maria.perez-page@manchester.ac.uk

Abstract

Pt and Pd, essential in diverse technologies yet limited in natural supply, necessitate sustainable recovery from secondary resources. Metallurgical approaches using deep eutectic solvents (DESs) offer greener and more selective routes for their extraction from acidic leachates. This study presents an integrated computational and experimental approach with new non-ionic DESs for the mutual separation of Pt(IV) and Pd(II) from model solutions via solvent extraction. New tri-n-octylphosphine oxide:carvacrol (TOCA) and lidocaine:carvacrol (LICA) DESs were developed. COSMO-RS predictions as well as DSC, and FT-IR characterisation confirmed the strong hydrogen-bonding interaction and non-ideal behaviour between the constituents of the mixtures. Extraction efficiency and selectivity in Pt and Pd separation were optimised under varying conditions (DES type and composition, and HCl concentration in the aqueous phase). TOCA demonstrated excellent selectivity for Pt(IV), with x_{TOPO} = 0.40, achieving 79.23% Pt and 18.74% Pd extraction efficiencies from 2 $mol.\,L^{-1}$ HCl, with a separation factor of 19.21. Conversely, LICA with x_{Lid} = 0.50 selectively extracted Pd (nearly complete) from 0.25 $mol.\,L^{-1}$HCl, with only 26.43% Pt co-extraction. FT-IR, UV-visible, and pH measurements suggested a neutral ion-pair association mechanism facilitated by proton co-extraction. Efficient back-extraction of metals using ethylenediaminetetraacetic acid for TOCA and acidified thiourea for LICA systems enabled solvent recyclability. TOCA maintained performance over five cycles, while LICA showed lidocaine leaching, indicating the need for rebalancing its composition to retain selectivity. These findings underscore the remarkable potential of carvacrol-based DESs as efficient media to close the loop of greener Pt and Pd separations.

Keywords: Platinum group metals; hydrometallurgy; DES; recyclability; metal separation; extraction mechanism, critical raw materials.

1. Introduction

Platinum group metals (PGMs), particularly platinum (Pt) and palladium (Pd), are indispensable in cutting-edge technologies owing to their high thermal and chemical stability, resistance to corrosion and oxidation, as well as superior catalytic efficiency in many reactions. Their widespread applications include three-way catalytic converters [1], diesel oxidation catalysts (DOC) [2], diesel particulate filter (DPF) [3], fuel cells [4], electrolysers [5], medical devices [6], and relevant industrial chemical reactions [7]. However, the global supply of PGMs is highly constrained, with the majority of known natural reserves concentrating in only a few countries, notably South Africa, Russia, Canada, and the United States [8]. In addition to the geopolitical implications deriving from their distribution, the extraction yields from natural ores are typically only a few grams per tonne [9], hence leading to the classification of PGMs as critical raw materials (CRMs) [10]. The forecasted demand for CRMs over the next two decades suggests 45% and 5% increases in Pd and Pt consumption, respectively, intensifying concerns about their long-term availability [11] and market price, currently surpassing $1,707/troy oz for Pt [12] and $1,277/troy oz for Pd [13].

At the same time, the environmental footprint of conventional mining practices, including hazardous waste generation and intensive solvent use, underscores the need to diversify sourcing strategies through urban mining by recovering PGMs from secondary resources, such as e-waste and industrial residues [14,15]. These waste streams offer a promising pathway for sustainable resource recovery while supporting material circularity [16], which companies including Umicore, BASF, Johnson Matthey, and Nippon PGM, are currently exploiting, although mainly based on conventional metal separation techniques [17]. Separation methods include conventional pyrometallurgy and hydrometallurgy, as well as more innovative approaches such as biometallurgy and solvometallurgy [18,19]. Pyrometallurgy shows severe disadvantages related to energy efficiency and hazardous chemical use and generation [20]. Biometallurgy capitalises on the metabolic activity of microorganisms, yet kinetic limitations are a notable constraint [21]. In contrast, hydrometallurgy, primarily involving sequential leaching and purification stages including solvent extraction (SX), effectively addresses the aforementioned limitations, showing good ability to process low-grade or complex waste streams, making it an efficient approach for PGM separation [22]. As part of SX operations, liquid–liquid extraction (LLX) in PGM refining typically involves the partitioning of metal ions from an acidic aqueous leachate into an organic phase, typically volatile organic solvents with almost no selectivity. Among these, alkyl sulfoxides, organophosphorus compounds, chloroform, hexane, and pyridine have been used, associated with significant environmental, health and safety (EHS) concerns [23]. These limitations underscore the need for more sustainable and selective solvents in PGM extraction technologies.

The development of solvometallurgy, a subfield of extractive metallurgy that employs non-aqueous or minimally aqueous solvents, has garnered increasing attention as a platform for selective metal separation [24]. Within this context, deep eutectic solvents (DESs) have emerged as versatile solvent systems, whose performance is governed by their composition and the nature of specific intermolecular interactions. DESs are increasingly recognised as chemically tunable solvent media, as their physicochemical characteristics, such as polarity, hydrogen-bonding ability, and solvation behaviour, can be tuned by varying the chemical nature and molar ratio of the hydrogen bond acceptor (HBA) and hydrogen bond donor (HBD) components [25–27]. In contrast to conventional organic diluents, DESs can accommodate substantially higher metal concentrations without solubility limitations or third-phase formation, thereby allowing through increased metal loading and reduced solvent-to-feed ratios. Furthermore, DESs eliminate the need for further diluents and complexing agents, while relying on simple component mixing rather than new chemical synthesis. This intrinsic design flexibility not only improves metal purity and extraction efficiency but also simplifies solvent regeneration and recyclability, supporting the development of more sustainable and scalable metal separation processes [28–30].

DESs have also shown promising applications in hydrometallurgy, where they have been used as extraction solvents for PGM recovery from aqueous leachates through LLX, as summarised in Table S1a [29], with comparable extraction performance indicators compared to ionic liquids and commercially implemented extractants, as shown in Table S1b. For instance, DESs composed of quaternary ammonium salts, such as trioctylmethylammonium chloride, combined with saturated carboxylic acids or alcohols (e.g., hexanoic acid, 1-hexanol) enabled the extraction of Pd(II) from highly acidic model solutions comprising common impurities (e.g., Cu, Ni, Fe, and Cr). The results showed that the enhanced Pd(II) extraction at low pH values was attributed to the predominance of $[PdCl_4]^{2-}$species [31]. Similarly, a tetraoctylammonium bromide:octanoic acid (1:2) DES achieved almost complete extraction of Pt(IV) (99.9%) and Pd(II) (99.7%) from wastewater, with minimal co-extraction of other metals, demonstrating high selectivity toward Pt and Pd over impurities [32]. Recently, a new class of DESs composed of non-ionic components has been highlighted due to their more favourable characteristics. These include lower viscosity, thereby facilitating better mass transport, lower water solubility, and superior phase disengagement, all of which are especially advantageous in LLX [29,33]. Tri-n-octylphosphine oxide (TOPO)-based DESs exemplify this trend, with systems such as TOPO:1-butanol (1:1) achieving up to 98.7% extraction efficiency (EE) for Pt(IV) from 1 $\mathrm{mol.\,L^{-1}}$ hydrochloric acid (HCl) solution. The DES also demonstrated recyclability over 4 cycles with efficient metal back-extraction using sodium hydroxide [34]. Further studies using TOPO:thymol (1:1) DES for selective separation of Pt(IV) and Pd(II) from chloride media consisting of various transition metal impurities

highlighted the tunability of extraction performance by acid concentration. Their findings revealed that while high acidity levels resulted in the highest EE, the greatest selectivity for PGMs over transition metal impurities was achieved at lower acidity. Additionally, selectivity toward Pt over Pd was observed, prompting subsequent studies focused solely on the individual separation of PGMs, which is a difficult task due to their similar properties and strong resistance to chemical transformation [33]. Vargas et al. investigated the selective separation of Pt(IV) from Pd(II) by optimising both experimental parameters and DES compositions. Under the identified conditions, the process achieved an EE of 63.10% for Pt(IV), while Pd(II) extraction remained low at 4.26%, demonstrating the potential of DESs for Pt–Pd discrimination [35]. Nevertheless, the extraction efficiency of the target metal (Pt) remained below 80%, indicating substantial Pt losses associated with achieving selectivity. Lidocaine (Lid)-based DESs have also shown effectiveness in precious metal recovery. A Lid:thymol (1:1) DES system extracted Au(III), Pd(II), and Pt(IV) from acidic leachate. Metal selectivity was strongly influenced by HCl concentration in the aqueous phase: at 2–3 $\mathrm{mol.\,L^{-1}}$ HCl, selective extraction of Au (97.8%) was achieved, while reduced HCl concentration (0.25–0.5 $\mathrm{mol.\,L^{-1}}$ HCl) favoured Pd and Pt extraction, with EE of 64.6% and 74.1%, respectively [36]. However, despite these promising recoveries, no selective separation between Pt and Pd was achieved, which is a key aspect.

Despite the promising progress in DES-based solvent extraction for PGM recovery, particularly using non-ionic DESs, most existing studies have primarily focused on the selective extraction of PGMs from base metals. In contrast, the more demanding task of achieving selective separation among individual PGMs, such as Pt and Pd, has received considerably less attention. This is commonly due to the chemical similarity of PGM chlorometalate species and the inherent difficulty of discriminating between them using conventional solvent systems [29]. Moreover, in the limited number of studies that report Pt–Pd selectivity, this improvement has often been accompanied by a reduction in extraction efficiency, resulting in low recovery of the target metal. Such compromised efficiency implies non-negligible losses of desired metal, highlighting a significant limitation for the practical application of current DES-based extraction systems. To date, only a limited number of studies have explored Pt-Pd selectivity using DESs, and these have typically addressed a single extraction preference, either favouring Pt over Pd or, less commonly, Pd over Pt under fixed conditions with low extraction efficiency [35,37]. However, no work has demonstrated mutual selectivity, the capability to preferentially extract Pt over Pd under one set of conditions, and conversely, to favour Pd over Pt under another set, while simultaneously maintaining high extraction efficiency for the target metal.

In addition, the extraction mechanisms governing Pt and Pd separation in DESs remain insufficiently understood. Most DES formulations have been developed empirically, without detailed mechanistic insight into the molecular-level interactions responsible for metal extraction and selectivity [29]. Such

understanding is essential for the rational design of DES compositions capable of discriminating between Pt and Pd chlorometalate species based on structure–interaction relationships rather than trial-and-error optimisation.

Comprehensive thermodynamic characterisation of DESs, including solid-liquid equilibrium (SLE) phase diagram, is of great importance for rational solvent design and extraction optimisation. In this regard, the Conductor-like Screening Model for Real Solvents (COSMO-RS) [38] provides a powerful tool to predict the SLE behaviour of non-ionic DESs, yielding high consistency with experimental measurements and offering great value for the design of new DESs [39]. Advancing individual PGM separation using DESs should also be accompanied by the development of reusable DESs to realise environmentally benign metallurgical processes.

Based on aforementioned gaps in the existing body of knowledge, this study investigates the design of novel DESs based on carvacrol (Carv), a biobased compound, particularly TOPO:carvacrol (TOCA) and lidocaine:carvacrol (LICA), supported by modelling and experimental analysis to develop efficient and selective systems for the mutual separation of Pt(IV) and Pd(II) from model hydrochloric acid solutions. These proposed systems eliminate the use of traditional organic solvents and complexing additives. A thorough characterisation of the DESs, including SLE phase diagrams and intermolecular interactions between constituents, is given. The key operating variables dictating extraction performance are systematically examined. Additionally, thermodynamic insights into the nature of the DES-metal interactions are given together with spectroscopic measurements to elucidate the extraction mechanisms. Finally, with an eye on solvent reuse to achieve circularity of prospective PGM recovery processes, a solvent regeneration strategy based on the back-extraction of Pt and Pd from the metal-loaded DESs is presented together with the reutilisation over multiple extraction–stripping cycles.

2. Methodology

2.1. Materials

Platinum(IV) chloride (CAS: 13454-96-1, 99%), Palladium(II) chloride (CAS: 7647-10-1, 99.995%), hydrochloric acid (CAS: 37 7647-01-0, 37%), thiourea (CAS: 62-56-6, 99%), ethylenediaminetetraacetic acid (EDTA, CAS: 60-00-4, 99%), and potassium thiocyanate (KSCN, CAS: 333-20-0, ≥99 %) were purchased from Sigma-Aldrich. DESs were prepared using tri-n-octylphosphine oxide (CAS: 78-50-2, ≥95%) from TCI and lidocaine (CAS: 137-58-6, 99%) from Bioserv as HBAs, and carvacrol (CAS: 499-75-2, 98%) supplied by Sigma-Aldrich as the HBD. A certified transition metal standard solution (Mix 3, 100 $mg.L^{-1}$ in 10% HCl) for ICP analysis was sourced from Supelco. Milli-Q water (resistivity 18.2 MΩ·cm) was used in all experiments. All reagents were utilised as received, except tri-n-

octylphosphine oxide, which was vacuum-dried (20 °C, 50 mbar) overnight due to its moderate hygroscopicity.

2.2. Computational methods

Determining the SLE phase diagram is a fundamental step in the judicious design of new DESs. Section S2 presents a short theoretical background on the thermodynamics behind the SLE of DESs. Herein, COSMO-RS was applied to predict the SLE behaviour of TOCA and LICA. The first step prior to COSMO-RS calculation was geometry optimisation and surface charge density calculations for TOPO, Carv, Pt- and Pd-chloro complexes with TmoleX2021 software using DFT level of theory with the BP86 functional, def2-TZVPD basis set, and the COSMO solvation model with FINE cavity [40]. Vibrational frequency analysis confirmed the stability of the optimised geometries. COSMOthermX software (version 18.0.2) and COSMObase database (version 15.0) were used to estimate the chemical potential (μ_i) of each component and finally conduct SLE predictions, assuming the availability of the melting point ($T_{m,i}$) and enthalpy of fusion ($\Delta_m H_i$) for each precursor [41,42]. Where melting property data were unavailable, the values were experimentally measured. The overall modelling workflow is illustrated in Fig. S1.

2.3. DES preparation

Binary mixtures of TOCA and LICA were prepared at various molar ratios, encompassing the entire molar composition range from 0.10 to 0.90 in increments of 0.10, as well as the commonly reported stoichiometric ratio of 0.33. All mixtures were prepared by mass using a Mettler Toledo New Classic MS analytical balance (standard uncertainty: u(m) = 0.0001g). The components were introduced into glass vials, which were immediately sealed with parafilm to minimise the potential of sublimation, evaporation, or moisture uptake. Each mixture was heated on a hot plate (IKA®, RCT basic) to a temperature above the melting point of the higher-melting precursor under continuous stirring of 500 rpm until a homogeneous liquid phase was created. The solvent was then stirred for one additional hour to ensure the formation of hydrogen bonds between the components. Following this, the mixtures were transferred to a dry heating block set at 25 °C and allowed to cool. The samples were then left undisturbed for 24 hours to assess their physical stability, confirming that no precipitation of any components in the mixture was observed.

2.4. DES characterisation

SLE phase diagrams were measured using differential scanning calorimetry (DSC 2500, TA instrument) under atmospheric pressure. Whenever glass transition temperatures were observed rather than melting points, the latter were visually determined by immersing the vial containing the mixture and

a stir bar in liquid nitrogen until complete solidification. The vial was then placed on a stirrer plate while continuously monitoring the temperature with a thermometer (Brannan −100/50 °C, standard uncertainty: *u*(T) = 0.1 °C). The moment when the stir bar began to move was considered the onset of melting [43]. Each measurement was conducted in triplicate, reporting the average value. FT-IR was employed to characterise the prepared DESs and their individual components, using a Bruker Vertex 70 spectrometer, to confirm the hydrogen-bonding interactions between the constituents. Experimental protocols are detailed in SI, section S3.1. and S3.2.

2.5. Metal extraction

2.5.1. LLX procedure

Stock solutions of HCl with varying concentrations (0.25–8 $\mathrm{mol.\,L^{-1}}$) were prepared volumetrically. Metal stock solutions were obtained by dissolving Pt(IV) chloride or Pd(II) chloride in water. To prepare mono- or bimetallic acidic feed solutions, the respective metal stock solutions were diluted in HCl to achieve a final metal concentration of 5 $\mathrm{mmol.\,L^{-1}}$, representing the typical concentration of metal investigated in the literature [29,44] and allowing its analytical quantification, and the desired HCl concentration. The resulting mixture was homogenised in an ultrasonic bath to ensure complete dissolution and uniform distribution. For LLX experiments, mono- or bimetallic acidic feed solutions were contacted with the selected DESs. The biphasic systems were prepared in centrifuge tubes at solvent-to-feed (S/F) ratios of 0.5 ($\mathrm{mL.\,mL^{-1}}$), unless stated otherwise. Each sample was subjected to mechanical mixing using a Labnet Vortemp 1550 shaker at 900 rpm and 25 °C (unless varied) for 60 min to ensure complete mass transfer. The different experimental conditions were then systematically varied to optimise extraction performance from single-metal solutions.

Subsequent phase separation was achieved by centrifugation at 5000 rpm for 10 min (Labnet Spectrafuge). The upper and lower phases were then separated and kept in a dry heating block (Labnet Accublock) set at a fixed temperature for sample analysis. The concentrations of Pt(IV) and Pd(II) in aqueous phase (raffinate) were determined using inductive coupled plasma with optical emission spectroscopy (ICP-OES) on a PlasmaQuant PQ 9000 Elite instrument (Analytik Jena, Germany), and the amount of metal in the DES phase (extract) was calculated by mass balance. All experiments were conducted in triplicate, and mean values with standard deviation (±σ) were reported. ICP-OES measurement is detailed in SI, section S3.3.

2.5.2. Evaluation of extraction performance

Extraction efficiency (EE), distribution ratio (D), and separation factor (SF) as performance indicators were calculated utilising the following equations:

$$\mathrm{EE_M}\ (\%) = \frac{\text{total mass of metal in extract phase}}{\text{total mass of metal in initial aqueous phase}} \times 100 \quad (1)$$

$$\mathrm{D_M} = \frac{\text{concentration of metal in extract phase}}{\text{concentration of metal in raffinate phase}} \quad (2)$$

$$\mathrm{D_M} = \frac{\mathrm{EE_M}\%}{100 - \mathrm{EE_M}\%} \times \frac{\mathrm{V_{raffinate\ phase}}}{\mathrm{V_{extract\ phase}}} \quad (3)$$

$$\mathrm{SF_{M1/M2}} = \frac{\mathrm{D_{M1}}}{\mathrm{D_{M2}}} \quad (4)$$

where the subscripts M_i refer to the metal being analysed, and V denotes the volume.

2.5.3. Extraction mechanism determination

To investigate the extraction mechanism and potential interactions between DES components and metal species, post-extraction samples were analysed using FT-IR and UV-visible spectrophotometry. FT-IR analysis was performed following a similar procedure outlined in SI, section S3.2, with spectra collected for the metal-loaded DES phases to evaluate shifts in functional group vibrations associated with metal–ligand interactions. UV-visible spectroscopy was employed to examine the coordination environment and speciation of Pt(IV) and Pd(II) complexes in both the initial aqueous phase and the post-extraction DES phases using a Shimadzu UV-2700 instrument. The protocol is detailed in SI, section S3.4.

2.6. Back-extraction and solvent recycling

Solvent regeneration through back-extraction was conducted to recover Pt and Pd from the metal-loaded DESs using various stripping reagents, including 0.2 $\mathrm{mol.L^{-1}}$ KSCN, 0.0005 $\mathrm{mol.L^{-1}}$ EDTA, 0.1 $\mathrm{mol.L^{-1}}$ thiourea in 0.5 $\mathrm{mol.L^{-1}}$ HCl (acidified thiourea), and Milli-Q water (resistivity 18.2 MΩ·cm). For the stripping process, the metal-loaded DES phases were mixed with each stripping reagent at a fixed extract-to-strip volumetric phase ratio of 0.5 ($\mathrm{mL.mL^{-1}}$) and agitated at 900 rpm for 60 min at 25 °C to facilitate complete metal transfer. Following the stripping step, the resulting aqueous phases (strip phases) were analysed by ICP-OES. The effectiveness of each stripping agent was evaluated based on the stripping efficiency (SE%), defined by equation (5):

$$\mathrm{SE_M}\ (\%) = \frac{\text{total amount of metal in strip phase}}{\text{total amount of metal in extract phase before stripping}} \times 100 \quad (5)$$

To evaluate the potential for long-term regeneration and reutilisation of the DESs, a series of extraction–stripping cycles were conducted under optimised conditions. Each experiment was performed in triplicate to confirm reproducibility. Additionally, the chemical integrity of regenerated

DESs was examined by FT-IR spectroscopy to verify structural stability of the solvents. The overall experimental procedure for this study is visualised in Fig. 1.

2.7. Mass-driven green metrics assessment

The transition toward environmentally responsible chemical design has led to the adoption of green chemistry principles, which aim to minimise or eliminate the use and generation of hazardous substances. Central to this approach is the use of green metrics, quantitative magnitudes that enable the systematic evaluation and comparison of the greenness of various extraction processes [45]. In this study, mass-based green metrics including process mass intensity (*PMI*), environmental factor ($E-factor$), solvent intensity (*SI*), and mass productivity (*MP* %) were calculated using equations (6) – (11).

$$PMI_{Pt,Pd} = \frac{\text{mass of acidic metal feed solution} + \text{mass of DES phase}}{\text{total mass of Pt(IV) and Pd(II) in extract phase}} \quad (6)$$

$$PMI_{Pt} = \frac{\text{mass of acidic metal feed solution} + \text{mass of DES phase}}{\text{total mass of Pt(IV) in extract phase}} \quad (7)$$

$$PMI_{Pd} = \frac{\text{mass of acidic metal feed solution} + \text{mass of DES phase}}{\text{total mass of Pd(II) in extract phase}} \quad (8)$$

$$E-factor = \frac{\text{total mass of Pt(IV) and Pd(II) in raffinate phase}}{\text{total mass of Pt(IV) and Pd(II) in extract phase}} \quad (9)$$

$$SI = \frac{\text{mass of DES phase}}{\text{total mass of Pt(IV) and Pd(II) in extract phase}} \quad (10)$$

$$MP\ (\%) = \frac{\text{total mass of Pt(IV) and Pd(II) in extract phase}}{\text{mass of acidic metal feed solution} + \text{mass of DES phase}} \times 100 \quad (11)$$

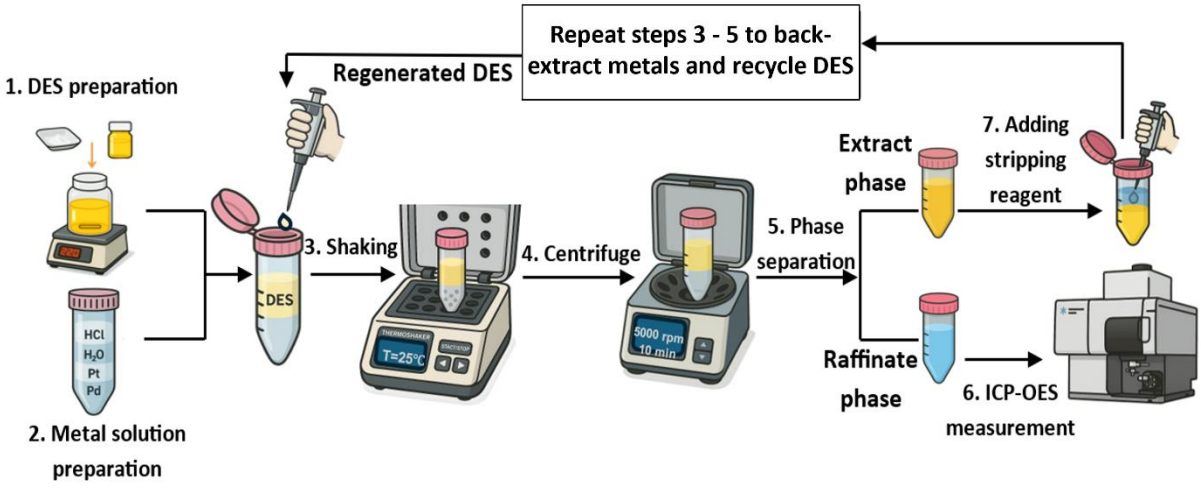

Fig. 1. Schematic of the experimental procedure for metal extraction and solvent recycling.

3. Results and Discussion

3.1. DES characterisation

3.1.1. Molecular optimisation of the precursors

A thorough evaluation of the SLE is critical to verify DES formation and to determine their practical liquid-phase operating range [46].

DFT calculations were conducted to optimise the molecular geometries of pure constituents (TOPO, Lid, and Carv), considering multiple conformers to identify the most energetically stable structure. The resulting σ-surfaces and σ-profiles, presented in Fig. 2(a), provided detailed information regarding the charge distribution on each molecule's surface: regions where $\sigma < -0.0082$ e.Å^{-2} correspond to HBD character, $\sigma > 0.0082$ e.Å^{-2} indicates HBA character, and $-0.0082 < \sigma < +0.0082$ e.Å^{-2} reflect non-polar character [47]. Analysis of σ-profiles indicated that TOPO and Lid exhibited prominent peaks only in the HBA region, reflecting the absence of hydrogen bond donor functionality and confirming their prominent role as HBA components in the DES formulation. In contrast, Carv displayed peaks in both the HBA and HBD regions but showed a stronger HBD capability, attributed to electron delocalisation and resonance effects of the oxygen of the hydroxyl group (–OH) (see Fig. 2(b)). This electronic configuration makes the oxygen atom a weaker hydrogen bond acceptor, thereby promoting hydrogen atom interactions with TOPO or Lid as HBA components of the proposed DESs [48].

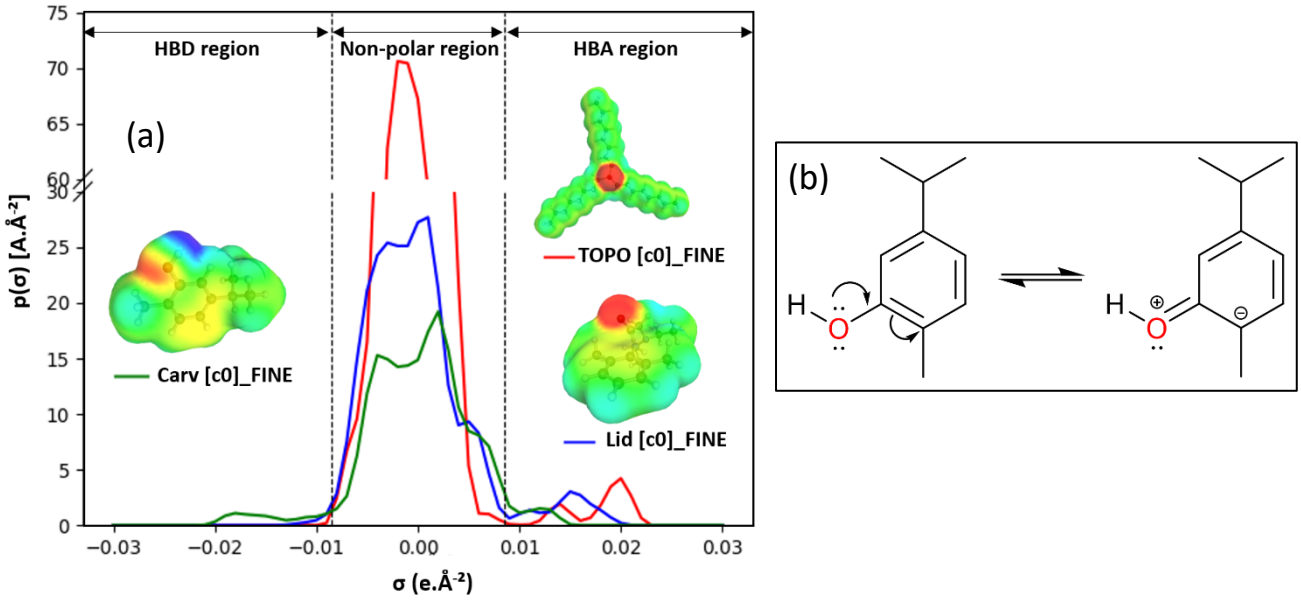

Fig. 2. (a) σ-surfaces and σ-profiles of the most stable conformer of TOPO (in red), Lid (in blue), and Carv (in green) using basis set of def2-TZVPD and COSMO solvation model with FINE cavity for DFT calculation; (b) Resonance structure of Carv.

3.1.2. SLE prediction by COSMO-RS and experimental validation

The SLE phase diagrams for TOCA and LICA were predicted using the COSMO-RS method. The obtained diagrams, depicted in Fig. 3, revealed clear eutectic points substantially lower than the ideal eutectic points and the individual component melting points, indicating strong negative deviations from thermodynamic ideality, which supports the formation of DESs rather than an eutectic solvent [49]. Distinct eutectic points were identified at x_{TOPO} = 0.31, T = –57.84 °C for TOCA and at x_{Lid} = 0.46, T = –98.42 °C for LICA. The yellow-shaded region in Fig. 3 denotes the concentration range where the DESs remained liquid at room temperature (25 ℃). This broad liquidus window enables precise adjustment of the physicochemical properties of DESs, facilitating metal extraction optimisation.

To validate COSMO-RS predictions, DSC was employed to experimentally assess the melting behaviour of mixtures across the full composition range. The melting properties of pure components (Carv, TOPO, and Lid) were also measured (Fig. S2(a), S2(l) and S2(w)) and compared with literature data (Table 1), confirming the accuracy of the DSC characterisation. From Fig. 3, a strong agreement was observed between COSMO-RS modelling and experimental measurements (DSC data and visual measurements), underscoring COSMO-RS as an effective predictive tool for the rational design and validation of new DESs.

Table 1. Comparison of experimentally determined melting properties of pure TOPO, Carv, and Lid with literature values at atmospheric pressure.

Compound	T_m (°C)		$\Delta_m H_i$ ($\mathbf{kJ.mol^{-1}}$)	
	this work	literature	this work	literature
TOPO	52.56	52.75[33]	44.84	58.02[33] and 39.00[43]
Carv	0.08	1.05[50]	10.59	11.49[50]
Lid	67.55	67.0[51]	14.74	15.30[51]

Journal Pre-proof

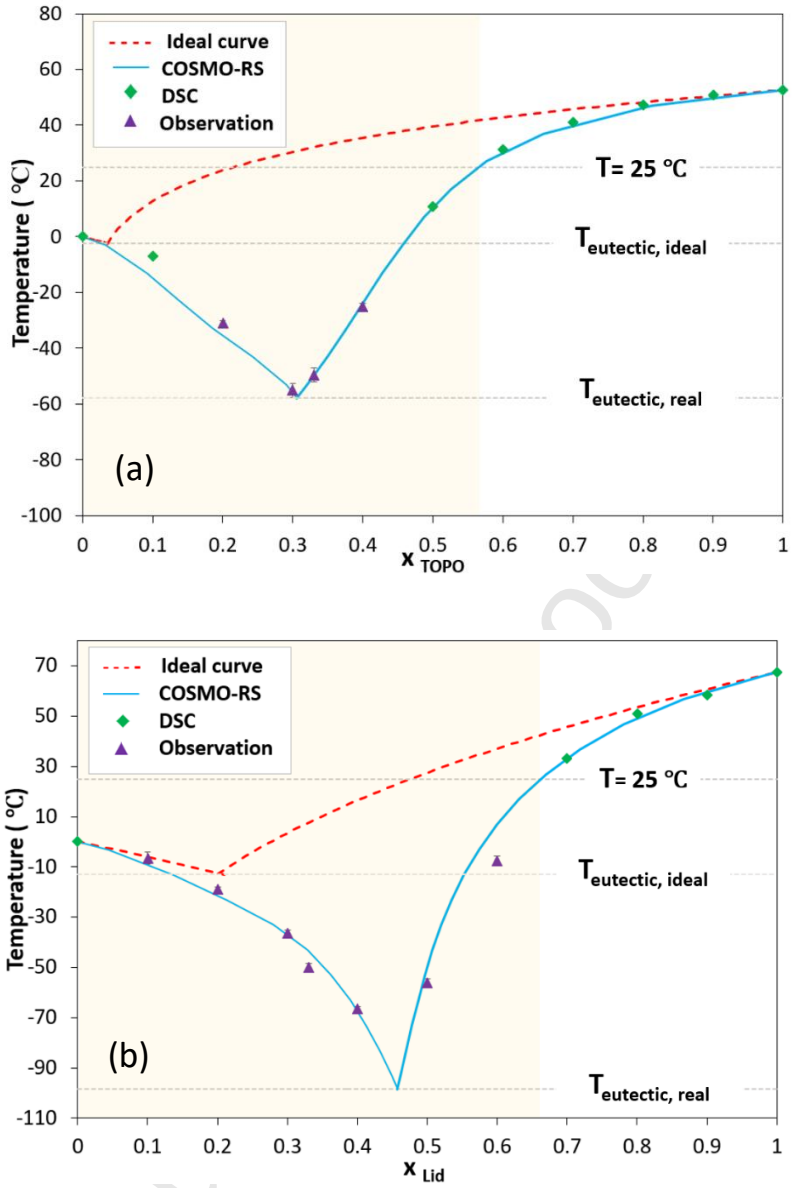

Fig. 3. SLE phase diagrams for (a) TOCA, (b) LICA. The yellow region indicates the liquidus range of the solvent at 25℃.

The DSC thermograms (Fig. S2) indicated that mixtures with x_{TOPO} = 0.10–0.40 (Fig. S2(b)-S2(f)) for TOCA and x_{Lid} = 0.10–0.60 (Fig. S2(m)-S2(s)) for LICA exhibited single endothermic events upon heating from –90 °C to 80 °C. However, within these composition ranges, the peak temperatures showed minimal variation, raising questions regarding whether these peaks represented true melting points or glass transitions [52]. Therefore, visual melting point determination was conducted to clarify this ambiguity, and the results are listed in Table S2. For instance, visual melting observations revealed that the DSC peak at –83.46 °C for the x_{TOPO} = 0.40 mixture corresponded more closely to a glass transition rather than an actual melting event, as the visual melting occurred at –25°C. Furthermore, no crystallisation peaks (exothermic events) were observed upon cooling back to –90 °C for these mixtures in DSC thermograms, suggesting metastable polymorph formation, a phenomenon

commonly encountered in non-ionic DESs, such as menthol-based systems, wherein annealing DSC or visual methods are recommended for accurate phase characterisation [48,50].

3.1.3. Analysis of the hydrogen-bonding interactions

To confirm the DES nature of TOCA and LICA solvents, the presence of intermolecular hydrogen bonding between HBA and HBD components is essential. Accordingly, FT-IR was employed to investigate hydrogen-bonding interactions of the DESs and their individual precursors. The FT-IR spectra of TOCA and TOPO and Carv, as shown in Fig. 4, exhibited no additional peaks for the prepared solvent compared with its pure components, suggesting that no chemical reaction occurred during its formation.

Characteristic vibrational bands of pure TOPO were identified (Fig. 4(a)) and found to be consistent with literature values [34]. Specifically, the P=O stretching vibration was observed at approximately 1144 cm^{-1}, accompanied by characteristic alkyl vibrations: –CH_3 (2952 cm^{-1}), –CH_2 asymmetric (2915 cm^{-1}), –CH_2 symmetric (2847 cm^{-1}), and -CH_2 scissoring (1466 cm^{-1}). Likewise, pure Carv exhibited distinct characteristic bands of its functional groups (Fig. 4(b)), including the broad phenolic O–H stretching band around 3358 cm^{-1} and a bending vibration at about 813 cm^{-1}. Additionally, bands corresponding to aromatic –CH stretching (3023 cm^{-1}), aliphatic –CH_2/–CH_3 stretching (2955, 2926, and 2868 cm^{-1}), aromatic C=C stretching (1589 cm^{-1}), C–O stretching (1262 cm^{-1}), aliphatic –CH_3 bending (1290 cm^{-1}), and aromatic –CH bending (808 cm^{-1}) were clearly observed and closely aligned with literature values [53].

Upon DES formation, a notable red shift with peak broadening in the O–H stretching band of Carv (from 3358 to 3161 cm^{-1}), as well as a slight red shift in the P=O stretching vibration of TOPO (from 1144 to 1139 cm^{-1}) was observed (Fig. 4(c)). These spectral changes indicated the formation of strong hydrogen bonding between the phenolic hydroxyl group of Carv and the phosphoryl oxygen of TOPO. The subtle shift in P=O vibration can be rationalised by the relatively rigid and strong dipole-dipole interaction in the P=O bond, limiting its susceptibility to vibrational displacement. In contrast, the prominent shift in the O–H stretching band is due to the longer bond, allowing hydrogen to vibrate easily and faster.

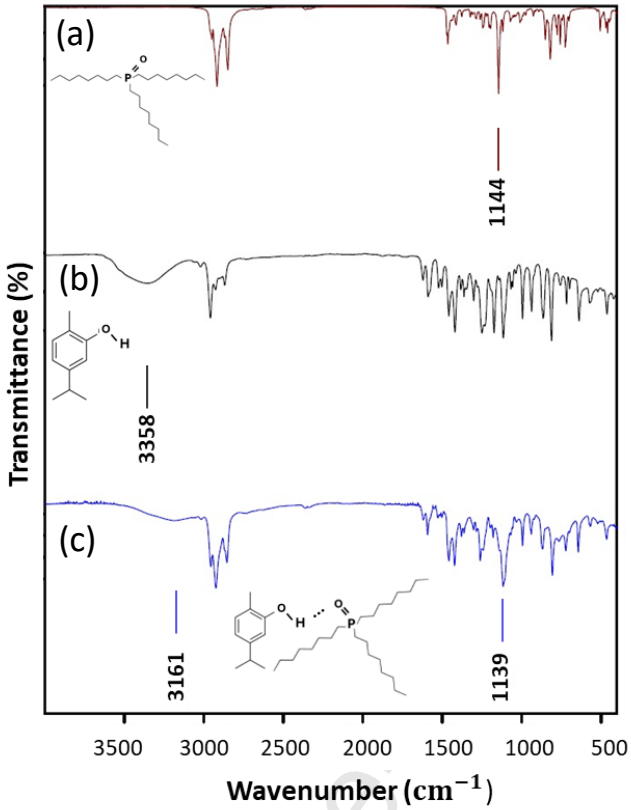

Fig. 4. FT-IR spectra of (a) pure TOPO, (b) pure Carv, and (c) TOCA mixture with $x_{TOPO} = 0.40$.

Similarly, FT-IR characterisation of the LICA mixture and its pure components (Lid and Carv) revealed no additional vibrational bands, supporting the absence of any chemical reaction between Lid and Carv (see Fig. 5). In the FT-IR spectrum of pure Lid (Fig. 5(b)), the characteristic stretching vibrations of the N–H and C=O functional groups were observed at 3247 and 1661 cm^{-1}, respectively. Additional bands corresponding to C–H stretching of the –CH_2 group (2967 cm^{-1}), aromatic C–H stretching (2918 and 2802 cm^{-1}), aromatic C=C stretching vibrations (1495 cm^{-1}), and C–N stretching (1595 cm^{-1}) were also present, in good agreement with literature data [54]. To investigate the formation of hydrogen bonding between Lid and Carv, particular attention was given to changes in the O–H, N–H, and C=O stretching vibrations. In pure Lid, intramolecular hydrogen bonding exists between the N–H and C=O groups. Upon DES formation, the phenolic O–H group of Carv preferentially interacted with the C=O group of Lid. This can be attributed to the higher electronegativity of oxygen (in the O–H group) compared to nitrogen (in the N–H group), making Carv a stronger HBD. This new O–H···O=C bond weakened the O–H bond in Carv, as electron density was partially drawn toward the C=O group, resulting in a pronounced red shift and broadening of the O–H stretching band (Fig. 5(c)). Concurrently, the amide C=O stretching band in Lid remained largely unchanged (from 1661 to 1662 cm^{-1}), suggesting that it is still engaged in strong hydrogen bonding, predominantly with carvacrol's O–H group rather than lidocaine's own N–H. As a result, the N–H bond is less involved in hydrogen bonding,

restoring more of its intrinsic bond strength, as reflected by a blue-shift of its stretching band (from 3247 to ~3273 cm^{-1}). In addition, a red-shift of the Carv O–H indicates stronger hydrogen bonding to Lid.

Overall, the combined evidence from FT-IR characterisation and SLE phase behaviour analysis confirmed the formation of true DESs in both TOCA and LICA mixtures.

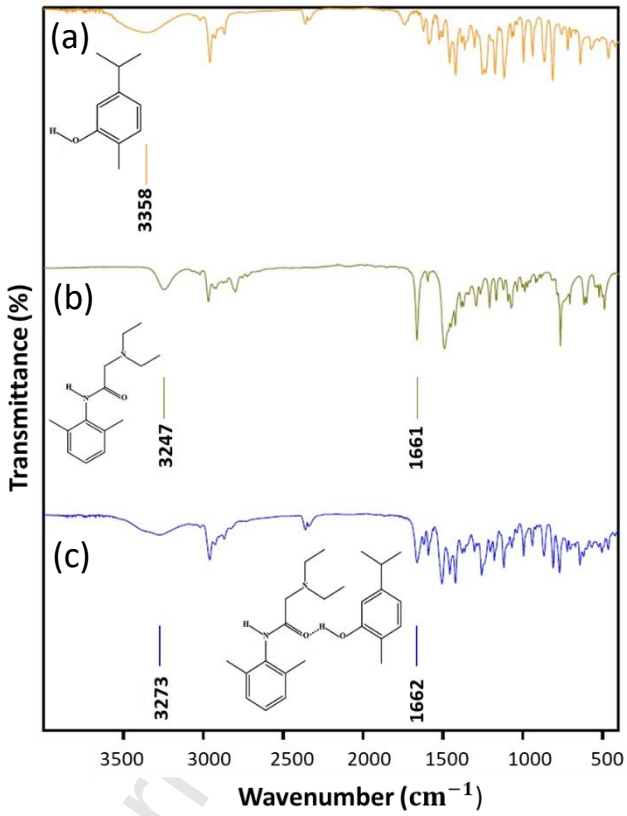

Fig. 5. FT-IR spectra of (c) pure Carv, (b) pure Lid, and (c) LICA mixture with $x_{Lid} = 0.50$.

3.2. Optimisation of metal extraction

3.2.1. Effect of DES nature and molar composition

To assess the effect of the changing properties of DESs with composition on extraction performance, a systematic investigation was conducted on the extraction efficiency and selectivity of Pt(IV) and Pd(II) from single-metal model solutions, employing Carv-based DESs formulated with TOPO and Lid as HBAs and different HBA:HBD molar ratios.

As depicted in Fig. 6, TOPO-based DESs consistently favoured the extraction of Pt(IV), whereas Lid-based systems achieved nearly complete extraction of Pd(II). These contrasting trends can be interpreted qualitatively using Pearson's Hard and Soft Acid and Base (HSAB) principle, where, in

simple terms, hard acids show a higher tendency to bind with hard bases and soft acids with soft bases. Thus, the HSAB theory relates the preferential stabilisation of metal–extractant associations to the relative hardness/softness of the metal centre and the interacting donor sites [55]. In concentrated chloride media, Pt and Pd are present predominantly as the chlorometalate complexes $[PtCl_6]^{2-}$and $[PdCl_4]^{2-}$, respectively, which differ in coordination geometry, charge density, and hydration strength. While both metals are classified as soft Lewis acids within Pearson's concept, Pd(II) is generally regarded as the softer and more polarisable centre, whereas Pt(IV) exhibits a higher effective charge and a more compact coordination environment [56]. In the present DES systems, metal extraction proceeds predominantly via protonation-assisted outer-sphere ion-pairing, further discussed in Section 3.3. From this perspective, the HSAB concept provides a qualitative guideline for understanding the preferential stabilisation of the respective chlorometalate complexes. The tertiary amine nitrogen of lidocaine, which is adjacent to an aromatic/amide group, is a borderline donor, with a partially delocalised lone pair; this gives it a relatively soft character and its association with the more polarisable Pd chlorometalate in the LICA system. In contrast, TOPO provides a strongly polar phosphoryl (P=O) group with hard acceptor character, which can more effectively stabilise the Pt chlorometalate ion pair environment in the TOCA DES, resulting in a higher apparent affinity for Pt(IV) under the investigated conditions [57,58].

Journal Pre-proof

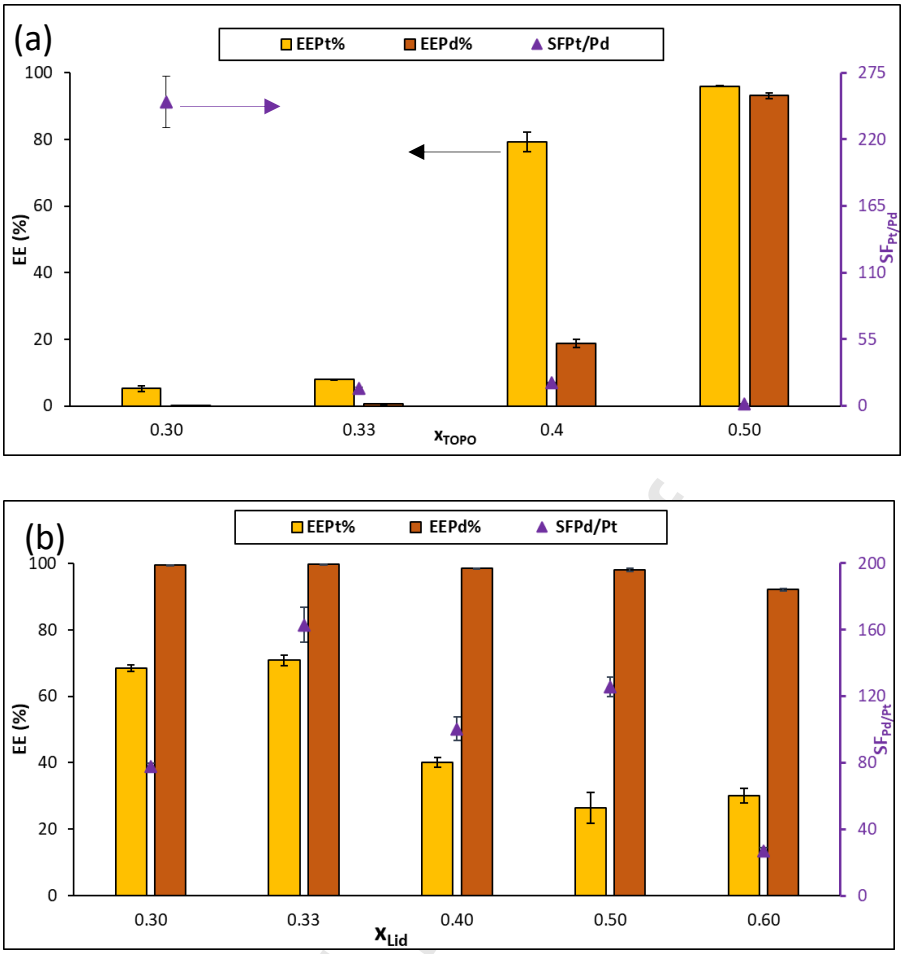

Fig. 6. Effect of HBA:HBD molar ratio on EE and selectivity (SF) for Pt(IV) and Pd(II) using (a) TOCA and (b) LICA. Conditions: $C_{Pt}^{aq} = 5\ \mathrm{mmol.\,L^{-1}}$; $C_{Pd}^{aq} = 5\ \mathrm{mmol.\,L^{-1}}$ in $C_{HCl}^{aq} = 2\ \mathrm{mol.\,L^{-1}}$ for extraction with TOCA and $C_{HCl}^{aq} = 0.25\ \mathrm{mol.\,L^{-1}}$ for extraction with LICA; at $\mathrm{S/F} = 0.5\ (\mathrm{mL.\,mL^{-1}})$; stirring speed $(\omega) = 900\ rpm$; $t = 5\ \mathrm{min}$; $T = 25\ °C$. All data in the figures are presented as mean values from three independent experiments (n=3), with error bars denoting the standard deviation (±σ). Error bars are included for all data; however, in some cases they are too small to be visually distinguished.

In the TOCA-based biphasic system, increasing the TOPO mole fraction ($\mathrm{x_{TOPO}}$) from 0.30 to 0.50 resulted in a significant improvement in the EE of both Pt and Pd, rising from 5.18% to 96.0% and from 0.02% to 93.1%, respectively. In contrast, when extracting with LICA, increasing the mole fraction of Lid ($\mathrm{x_{Lid}}$) led to a notable decrease in Pt EE, from 70.78% at $\mathrm{x_{Lid}}$ = 0.33 to 26.43% at $\mathrm{x_{Lid}}$ = 0.50, while Pd extraction remained consistently high (>92%) across all molar ratios examined. This contrasting behaviour highlights the non-linear and system-dependent influence of HBA:HBD molar stoichiometry, which can be attributed to the differences in eutectic composition and hydrogen-bonding environments between the two DES systems.

To clarify the role of Carv, its direct contribution to extraction performance was examined. Under fixed experimental conditions, pure Carv exhibited negligible metal partitioning (EE_{Pt} < 2% and D value of 0.01), suggesting that the extraction capability of DESs arises predominantly from the HBAs (TOPO or Lid). Nevertheless, the pronounced effect of varying the HBA:HBD molar ratio indicates that Carv exerts a significant indirect influence by modulating the Carv–HBA hydrogen-bonding network, which in turn governs key physicochemical properties of the DES phase, including polarity, microstructural organisation, and the ability to accommodate protons and metal–chloro complexes. This interpretation is supported by the SLE phase diagrams (Fig. 3), which show that x_{TOPO} = 0.30 for TOCA and x_{Lid} = 0.50 for LICA are the closest experimentally investigated compositions to the predicted eutectic points. At these compositions, the hydrogen-bonding interactions between the HBA and HBD are at their strongest, favouring the formation of structurally robust DES phases and avoiding third-phase generation even under harsh acidic conditions. This is a notable advantage, as third-phase formation commonly limits non-ionic extractants in conventional SX systems [35,59]. However, such rigidity in the DES network limits the structural rearrangements required for proton incorporation and effective coordination with metal-chloro complexes, creating higher energetic barriers and thereby diminishing extraction performance. This behaviour reflects a mechanistic antagonism between the strength of intermolecular interactions within the DES phase and the efficiency of SX, a relationship previously proposed by Vargas et al., further discussed in Section 3.3 [35].

To assess extraction selectivity, the conventional separation factor (SF) was employed. For the TOPO-based DESs, the highest $SF_{Pt/Pd}$ value (250.78) was observed at x_{TOPO} = 0.30; however, the corresponding extraction efficiencies for both Pt and Pd were extremely low (EE ≤ 5 %). This highlights the inherent limitations of SF in capturing (i) operationally practical extraction efficiency of desired metal, and (ii) greater difference between the extraction efficiencies of a target metal and its competing counterparts. These limitations become particularly evident when the D values of both metals are either very low (close to zero) or extremely high (near-complete extraction) [35]. In such cases, SF may be artificially amplified or suppressed because it is defined as a ratio of D values, while D itself is a non-linear function of EE, as described in equation (3). More specifically, the high $SF_{Pt/Pd}$ obtained at $x_{TOPO} = 0.30$ arises from very low D values for both Pt and Pd ($D_{Pt} = 0.109$ and $D_{Pd} = 0.0004$). Under these conditions, small absolute differences in D can lead to disproportionately large SF values, even though the corresponding EEs are extremely low and of limited practical relevance ($EE_{Pt} = 5.18\%$ and $EE_{Pd} = 0.02\%$). Therefore, in this study, selectivity was evaluated by jointly considering SF, the absolute extraction efficiency of target metal, and the magnitude of the difference between EE_{Pt} and EE_{Pd}. On this basis, $x_{TOPO} = 0.40$ was identified as the optimal composition for

the TOCA system, offering high Pt selectivity with operationally relevant Pt extraction efficiency (79.23%).

A similar behaviour was observed for the LICA system. The highest $SF_{Pt/Pd}$ (163.05) was obtained at $x_{Lid} = 0.33$ due to the near-complete extraction of Pd ($EE_{Pd} = 99.75\%$), corresponding to a very high D_{Pd} (792.43), although this composition also yielded the highest Pt extraction efficiency among the studied compositions ($EE_{Pt} = 70.78\%$ and $D_{Pt} = 4.86$). Accordingly, $x_{Lid} = 0.50$ was selected as the optimal composition for the LICA system, as it provides superior Pd separation performance by achieving high Pd recovery ($EE_{Pd} = 98.03\%$ and $D_{Pd} = 103.03$) while effectively suppressing Pt co-extraction ($EE_{Pt} = 26.43\%$).

These results also highlight a trade-off between extraction efficiency and selectivity [35,60]. In the TOCA system, x_{TOPO} = 0.50 yielded the highest EE for both Pt and Pd, but with poor selectivity. Conversely, x_{TOPO} = 0.40 offered a more balanced outcome, substantial Pt extraction with minimal Pd co-extraction. A comparable pattern was observed in Lid-based systems, where x_{Lid} = 0.33 facilitated greater extraction of both metals, while x_{Lid} = 0.50 favoured Pd selectivity.

Overall, these results underscore the importance of carefully optimising the DES compositions to tailor solvent structure and function, either to maximise EE or enhance selectivity, depending on the desired separation outcome. Accordingly, TOCA with x_{TOPO} = 0.40 and LICA with x_{Lid} = 0.50 were identified as the optimal DESs and compositions for the efficient and selective extraction of Pt and Pd, respectively.

3.2.2. Effect of aqueous HCl concentration

Hydrochlorination, involving dissolution in HCl with an oxidising agent, is among the most common methods for leaching platinum-bearing ores and secondary resources. Accordingly, Pt and Pd extraction from HCl solutions represents a relevant and practical model system [32]. The aqueous HCl concentration plays a pivotal role in determining metal speciation and governing the metal–extractant complexation, both critical to achieving efficient extraction. To explore this effect, the extraction behaviour of Pt and Pd from separate single-metal HCl solutions was examined over the concentration range of 0.25 to 8 $\mathrm{mol.\,L^{-1}}$, commonly employed in hydrochlorination [61].

In the TOCA system (Fig. 7(a)), increasing the HCl concentration up to 6 $\mathrm{mol.\,L^{-1}}$ markedly enhanced the EE of both metals. Pt EE increased sharply from 36.26% to 95.47%, while Pd showed a gradual increase from 11.75% to 37.75%. However, further increasing the HCl concentration to 8 $\mathrm{mol.\,L^{-1}}$ resulted in a slight decrease in Pt EE to 92.29% and a more pronounced decline in Pd EE to 29.94%, respectively. These results indicate that relatively high proton activity initially promotes extraction by facilitating metal–extractant complexation, whereas excessively high HCl concentrations can hinder

extraction, which is most likely due to competition between free chloride ions and PGM–chloro complexes for coordination with the extractant. Prior work reported a comparable trend, where extraction suppression was observed upon increasing HCl concentration. To further confirm the competitive effect of chloride anion in that study, NaCl was also introduced into the initial aqueous phase over the same concentration range as HCl, yielding a similar suppression pattern [36].

To determine the optimum HCl concentration for achieving the greatest selectivity toward Pt over Pd using TOCA (x_{TOPO} = 0.40), $SF_{Pt/Pd}$ was calculated over the studied range of HCl concentrations. It was shown that the $SF_{Pt/Pd}$ peaked at 34.77 at $C_{HCl}^{aq} = 6\ \mathrm{mol.\,L^{-1}}$. However, considering environmental impact, industrial practicality and, most importantly, the maximum difference in EE between Pt and Pd, a concentration of $C_{HCl}^{aq} = 2\ \mathrm{mol.\,L^{-1}}$ was identified as optimal for the efficient and selective recovery of Pt over Pd using TOCA.

A similar trend was observed for LICA (x_{Lid} = 0.50) (Fig. 7(b)). Increasing HCl concentration up to 2 $\mathrm{mol.\,L^{-1}}$ significantly boosted Pt EE from 26.43% to 94.61%, followed by a decrease to 81.3% at $C_{HCl}^{aq} = 6\ \mathrm{mol.\,L^{-1}}$. In contrast, Pd EE remained nearly complete and constant up to 1 $\mathrm{mol.\,L^{-1}}$, after which it gradually declined to 61.33% at $C_{HCl}^{aq} = 6\ \mathrm{mol.\,L^{-1}}$. Notably, the highest selectivity ($SF_{Pd/Pt} = 125.35$) was achieved at low acidity ($C_{HCl}^{aq} = 0.25\ \mathrm{mol.\,L^{-1}}$), where Pd was extracted approaching completion, while Pt EE remained below 30%. Hence, $C_{HCl}^{aq} = 0.25\ \mathrm{mol.\,L^{-1}}$ was identified as the optimal acidity level for achieving efficient and selective extraction of Pd over Pt using LICA.

These findings indicate that increasing C_{HCl}^{aq} initially enhances the extraction of Pt(IV) and Pd(II) by (i) stabilising their speciation in aqueous phase, predominantly as the anionic chlorometalate complexes ($[PtCl_6]^{2-}$and $[PdCl_4]^{2-}$), and (ii) facilitating metal–extractant complexations through acid co-extraction. Proton transfer into the DES modifies its structure and hydrogen-bond network to provide the counter-ions needed for the extraction of these anionic chlorometalate complexes. However, at higher C_{HCl}^{aq}, the rising chloride activity introduces competitive interactions that reduce the affinity of the extractant for the target metal complexes, diminishing overall extraction performance [62,63].

Among the studied metal complexes, $[PtCl_6]^{2-}$displayed consistently high extraction performance across a broad range of HCl concentrations, owing to its high chemical stability and low susceptibility to hydrolysis. Its extraction declined only under extremely low or excessively high HCl concentrations. In contrast, $[PdCl_4]^{2-}$was more sensitive to variations in acidity and chloride concentration, reflecting its moderate hydrolysis tendency and stronger competition with free chloride ions. This greater sensitivity led to a more pronounced decrease in Pd EE under harsh acidic conditions [64].

Collectively, these observations underscore the importance of fine-tuning both the C_{HCl}^{aq} and the DES composition to achieve efficient mutual separation of Pt and Pd.

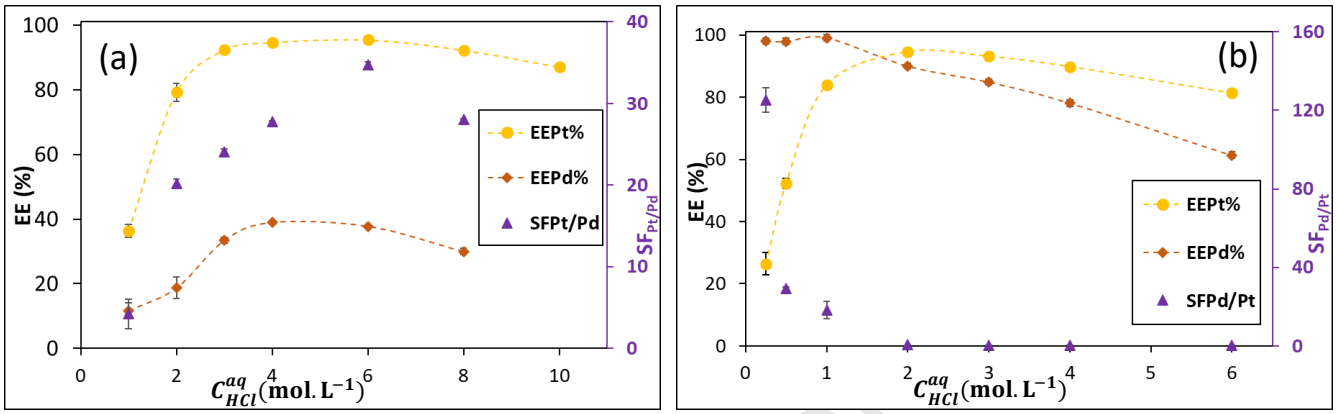

Fig.7. Effect of aqueous HCl concentration on EE and selectivity (SF) for Pt(IV) and Pd(II) using (a) TOCA ($x_{TOPO} = 0.40$) and (b) LICA ($x_{Lid} = 0.50$). Conditions: $C_{Pt}^{aq} = 5\ \mathrm{mmol.L^{-1}}$; $C_{Pd}^{aq} = 5\ \mathrm{mmol.L^{-1}}$; $S/F = 0.5\ (\mathrm{mL.mL^{-1}})$; $\omega = 900\ rpm$; $t = 5\ \mathrm{min}$; $T = 25\ ^{\circ}C$. The symbols represent experimental data points, while the dashed lines are provided solely as visual guides. All data points in the figures are presented as mean values from three independent experiments (n=3), with error bars denoting the standard deviation (±σ). Error bars are included for all data points; however, in some cases they are too small to be visually distinguished.

3.2.3. Effect of solvent-to-feed volumetric phase ratio

The volume of DES used as the extractant is a key parameter in metal recovery processes, influencing not only economic considerations such as solvent cost, but also environmental sustainability and resource utilisation. It also influences the enrichment factor, defined as the ratio of the target metal ion concentration in the extract phase to that in the initial feed, crucial for recovering trace metals from low-grade secondary resources [32,65]. In light of this, the effect of solvent-to-feed volumetric phase ratio (S/F) on Pt(IV) and Pd(II) extraction performance was examined. As illustrated in Fig. 8(a) and 8(b), increasing S/F enhanced the overall EE of both metals, but significantly reduced system selectivity. This trend can be attributed to the increased availability of extractant molecules at higher DES loads, which increases the number of accessible coordination sites for metal complexation. As a result, the competition between metal ions for binding sites is reduced, facilitating more efficient transfer of both metals into the DES phase. More specifically, in the TOCA-based biphasic system, increasing S/F from 0.5 to 1 and 2 $(\mathrm{mL.mL^{-1}})$ resulted in a slight increase in Pt EE (approximately 5%), whereas Pd EE increased sharply from 18.74% to 26.78% and 34.99%, respectively. This led to a substantial decline in the $SF_{Pt/Pd}$, dropping to 11.25 (Fig. 8(a)). A similar trend was observed when separating with LICA, where rising S/F to 1 and 2 $\mathrm{mL.mL^{-1}}$ reduced the $SF_{Pd/Pt}$ from 125.35 to 72.90 and 45.69, respectively, due to a near two-fold increase in Pt EE (reaching 49.56%), while Pd extraction

remained largely unaffected by volumetric phase ratio variation in LICA-based systems, as shown in Fig. 8(b).

Given environmental considerations, such as minimising solvent consumption, and recognising that increasing the DES volume provided only marginal improvements in the EE of the target metal while substantially compromising selectivity, an S/F of 0.5 $\mathrm{mL.\,mL^{-1}}$ was selected as the optimal condition for further investigations. This approach aligns with the first and second principles of green chemistry, namely the prevention of waste and the maximisation of material efficiency, by reducing excess DES use and ensuring more effective incorporation of input materials into the desired extraction process [66].

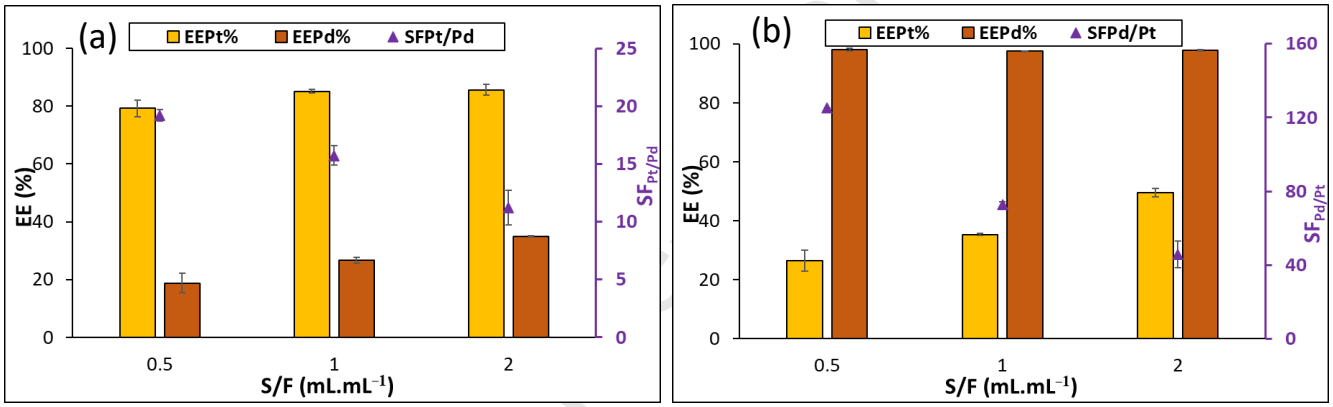

Fig. 8. Effect of S/F on EE and selectivity (SF) for Pt(IV) and Pd(II) using (a) TOCA ($\mathrm{x_{TOPO}} = 0.40$) and (b) LICA ($\mathrm{x_{Lid}} = 0.50$). Conditions: $C_{Pt}^{aq} = 5\ \mathrm{mmol.\,L^{-1}}$; $C_{Pd}^{aq} = 5\ \mathrm{mmol.\,L^{-1}}$ in $C_{HCl}^{aq} = 2\ \mathrm{mol.\,L^{-1}}$ for extraction with TOCA and $C_{HCl}^{aq} = 0.25\ \mathrm{mol.\,L^{-1}}$ for extraction with LICA; $\omega = 900\ rpm$; $t = 5\ \mathrm{min}$; $T = 25\ °C$. All data in the figures are presented as mean values from three independent experiments (n=3), with error bars denoting the standard deviation (±σ). Error bars are included for all data; however, in some cases they are too small to be visually distinguished.

Moreover, the effect of contact time, ranging from 5 to 480 min, on Pt and Pd extraction efficiencies using TOCA and LICA was evaluated under the controlled laboratory operating conditions employed in this study. As shown in Fig. S3, thermodynamic equilibrium was achieved within 5 min for both systems, and EE remained stable over time, indicating the absence of mass transfer limitations under these experimental conditions.

3.2.4. Effect of temperature and thermodynamic assessment

The influence of temperature on the extraction behaviour and partitioning of Pt(IV) and Pd(II) in both Carv-based DESs was examined over the range of 15 °C to 50 °C, remaining below the onset degradation temperatures. As illustrated in Fig. 9(a), increasing the temperature when extracting with TOCA led to a pronounced decline in EE for both metals. Specifically, Pt EE dropped from 83.09% at

15 °C to 61.40% at 50 °C, while Pd EE declined from 19.01% to 10.06%. The selectivity to Pt, expressed by $\mathrm{SF}_{\mathrm{Pt/Pd}}$, also decreased from 20.98 to 14.14, indicating a temperature-induced reduction in extraction preference for Pt over Pd. Although the highest Pt EE and selectivity were observed at 15 °C, a temperature of 25 °C was selected for subsequent experiments due to the associated energy requirements to cooling and the relatively minor performance difference between 15 °C and 25 °C. Operating at 25 °C also aligns with the sixth principle of green chemistry, which advocates for the design of processes under ambient conditions to reduce energy consumption related to heating or cooling, thereby enhancing the overall sustainability of the extraction system.

In contrast, the LICA-based system showed an opposite trend (Fig. 9(b)). At 15 °C, the extract phase formed an emulsion-like mixture, making phase disengagement very difficult. Rising the temperature from 25 °C to 50 °C resulted in only a slight decline in Pd recovery, from 98.03% to 94.84%, but more than a two-fold increase in Pt EE. However, this improvement in Pt recovery came at the expense of selectivity; the $\mathrm{SF}_{\mathrm{Pd/Pt}}$ dropped dramatically from 125.35 to 14.24. Therefore, 25 °C was selected as the optimal operating temperature for Pd extraction using LICA, offering a balance between extraction efficiency, selectivity, and phase stability.

To gain further insight into the thermodynamic driving forces underlying these trends, the standard Gibbs free energy change (*ΔG°*), standard enthalpy change (*ΔH°*), and standard entropy change (*ΔS°*) were calculated using the van 't Hoff approach (equations (12) – (14)) based on the temperature dependence of the distribution ratio [64].

$$ln(D) = \frac{-\Delta H^{\circ}}{RT} + \frac{\Delta S^{\circ}}{R} \quad (12)$$

$$\Delta G^{\circ} = -RT\, ln(D) \quad (13)$$

$$\Delta G^{\circ} = \Delta H^{\circ} - T\Delta S^{\circ} \quad (14)$$

where *D* is the distribution ratio, *T* stands for temperature (K), and *R* is the universal gas constant (8.314 $\mathrm{J.mol^{-1}.K^{-1}}$). The corresponding thermodynamic parameters are visualised in Fig. 9(c) and 9(d), with the calculated values in Table S3.

Using TOCA for extraction, the *ΔG°* values for Pt were consistently negative across the tested temperature range, indicating a spontaneous Pt extraction process. In contrast, *ΔG°* values for Pd were positive, confirming the thermodynamically unfavourable nature of Pd extraction under the same experimental conditions. Both Pt and Pd exhibited negative *ΔH°* and *ΔS°* values, implying that the extraction is exothermic and accompanied by a decrease in system entropy, consistent with the

formation of more ordered metal-extractant complexes. These findings align with the observed decrease in EE at elevated temperatures.

Conversely, in the LICA system, Pt extraction was characterised by a positive $\Delta H°$ (41.87 kJ.mol^{-1}) and $\Delta S°$ (0.14 kJ.mol^{-1}.K^{-1}), indicating an endothermic process. While $\Delta G°$ for Pt was slightly positive at 298 K, it decreased with increasing temperature, supporting the experimentally observed enhancement in EE. Pd extraction, on the other hand, showed negative $\Delta G°$ (–11.47 kJ.mol^{-1}) and $\Delta H°$ (–27.88 kJ.mol^{-1}), confirming a spontaneous and exothermic Pd extraction process. These results further validate the greater efficiency and selectivity of Pd extraction by LICA at moderate temperatures.

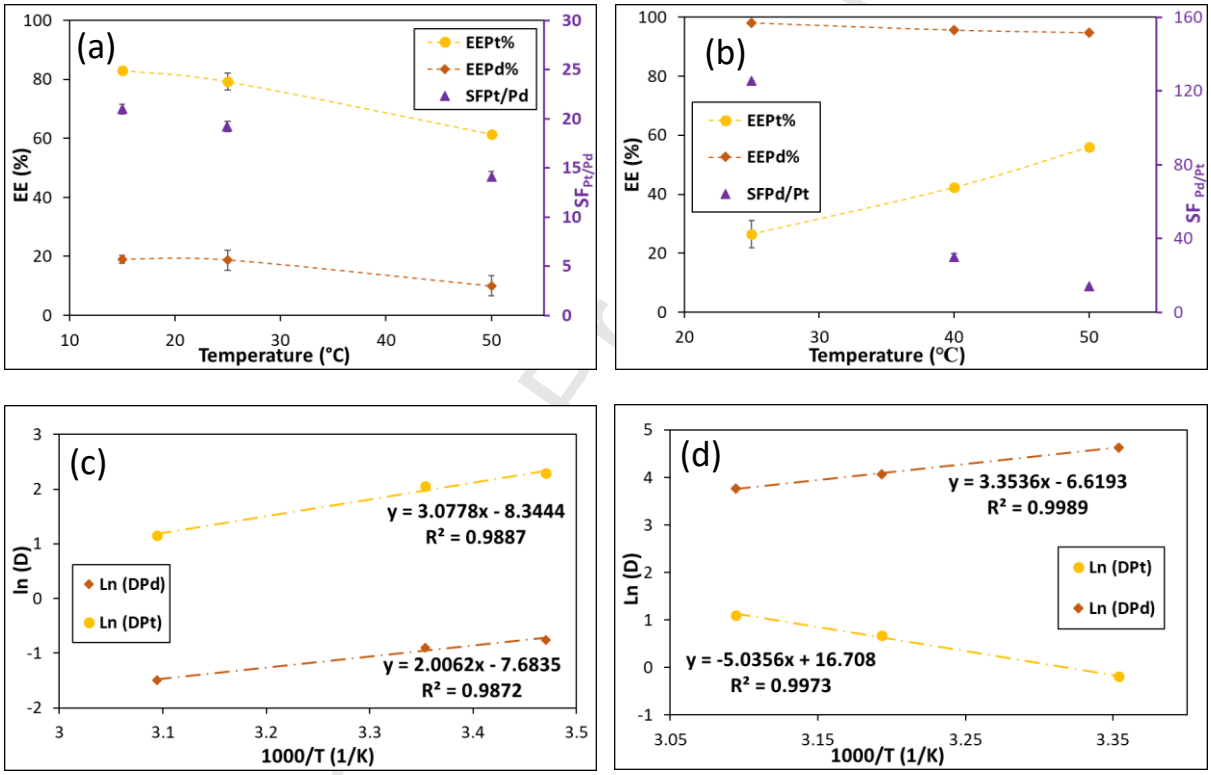

Fig. 9. Effect of temperature on EE and selectivity (SF) for Pt(IV) and Pd(II) using (a) TOCA ($x_{TOPO} = 0.40$) and (b) LICA ($x_{Lid} = 0.50$); corresponding van 't Hoff plots for (c) TOCA ($x_{TOPO} = 0.40$) and (d) LICA ($x_{Lid} = 0.50$). Conditions: $C_{Pt}^{aq} = 5$ mmol. L^{-1} ; $C_{Pd}^{aq} = 5$ mmol. L^{-1} in $C_{HCl}^{aq} = 2$ mol. L^{-1} for extraction with TOCA and $C_{HCl}^{aq} = 0.25$ mol. L^{-1} for extraction with LICA; $S/F = 0.5$ (mL. mL^{-1}); $\omega = 900\ rpm$; $t = 5$ min; The symbols represent experimental data points. Dashed lines in (a) and (b) serve solely as visual guides, while those in (c) and (d) represent the linear regression fittings. All data points in the figures are presented as mean values from three independent experiments (n=3), with error bars denoting the standard deviation (±σ). Error bars are included for all data points; however, in some cases they are too small to be visually distinguished.

To complement the experimental thermodynamic analysis, COSMO-RS modelling was employed using quantum-chemically optimised molecular structures of each molecule and their respective metal cavities. This approach was used to estimate the excess Gibbs free energy (G^E) and excess enthalpy (H^E) associated with the solvation of the metal chloro-complexes in the aqueous and DES phases. These excess properties quantify deviations from ideal behaviour and therefore provide insights into the relative stabilisation of the solutes in each solvent environment. In this framework, more negative H^E values suggest stronger solute–solvent interactions, while more negative G^E values show the spontaneity of the process and reflect more thermodynamically favourable incorporation of the anionic metal complex into the solvent phase [47]. Accordingly, H^E and G^E values were estimated for $[PtCl_6]^{2-}$and $[PdCl_4]^{2-}$ in both DES and aqueous phases at 25 °C, assuming a solute mole fraction of 0.001 to ensure no precipitation effects are involved (Table 2).

For TOCA, $[PtCl_6]^{2-}$exhibited slightly more favourable interaction with the DES phase than $[PdCl_4]^{2-}$, as indicated by a marginally more negative ΔG^E (–4.6065 vs. –4.5853 $kJ.mol^{-1}$) and ΔH^E (–8.6813 vs. –8.6623 $kJ.mol^{-1}$), consistent with the experimental preference for Pt(IV). Conversely, using LICA, $[PdCl_4]^{2-}$displayed a slightly more negative ΔG^E (–3.0200 $kJ.mol^{-1}$) than $[PtCl_6]^{2-}$(–3.0193 $kJ.mol^{-1}$), suggesting preference for Pd(II) extraction. These thermodynamic trends align with experimental observations, highlighting the reliability of COSMO-RS in predicting metal–solvent interactions and extraction selectivity.

Table 2. COSMO-RS predictions of excess enthalpy (H^E) and excess Gibbs free energy (G^E) for $[PtCl_6]^{2-}$ and $[PdCl_4]^{2-}$ in Carv-based DESs and aqueous HCl solutions at solute mole fraction of 0.001 and 25 °C.

System	H^E $(kJ.mol^{-1})$	G^E $(kJ.mol^{-1})$
$[PtCl_6]^{2-}$@ TOCA ($x_{TOPO} = 0.40$)	–9.4736	–4.9144
$[PtCl_6]^{2-}$@ $C_{HCl}^{aq} = 2\ mol.L^{-1}$ HCl	–0.7922	–0.3079
$[PdCl_4]^{2-}$@ TOCA ($x_{TOPO} = 0.40$)	–9.4753	–4.9141
$[PdCl_4]^{2-}$@ $C_{HCl}^{aq} = 2\ mol.L^{-1}$ HCl	–0.8129	–0.3289
$[PtCl_6]^{2-}$@ LICA ($x_{Lid} = 0.50$)	–7.1800	–3.2497
$[PtCl_6]^{2-}$ @ $C_{HCl}^{aq} = 0.25\ mol.L^{-1}$ HCl	–0.2966	–0.2304
$[PdCl_4]^{2-}$@ LICA ($x_{Lid} = 0.50$)	–7.2048	–3.2713
$[PdCl_4]^{2-}$@ $C_{HCl}^{aq} = 0.25\ mol.L^{-1}$ HCl	–0.3165	–0.2513

3.2.5. Comparative analysis of single-metal and binary-metal solutions

Several studies have demonstrated that PGM extraction behaviour can vary with matrix complexity (i.e., single-metal, binary-metal, or multi-metal solutions). For instance, Ru(IV) has been reported to modify the coordination environment of Ir(IV), thereby enhancing its affinity toward Cyanex® 923 [67]. To evaluate the applicability and robustness of the studied DESs under more realistic conditions, particularly given the well-documented challenge of separating Pt and Pd due to their similar physicochemical properties, a systematic comparison was conducted between the extraction behaviour of Pt(IV) and Pd(II) in mono- and bimetallic solutions. As shown in Fig. 10(a), introducing a second metal when TOCA is used for extraction had no appreciable effect on extraction efficiency or the separation factor, suggesting no mutual interference between Pt and Pd. These results indicate that the extraction performance observed in single-metal systems is transferable to more complex matrices. Accordingly, the consistent extraction efficiency and Pt selectivity observed in binary Pt–Pd solutions corroborate the reliability of TOCA (x_{TOPO} = 0.40), even in the presence of equimolar Pd.

In contrast, LICA (x_{Lid} = 0.50) exhibited a clear deviation in selectivity when transitioning from single-metal to bimetallic feeds (Fig. 10(b)). Although the EE of Pt and Pd were largely unchanged, the $SF_{Pd/Pt}$ notably decreased in the binary system. This reduction is attributed to the partial leaching of DES components into the aqueous phase (Table S4), which perturbs the distribution equilibrium and alters metal partitioning. Despite this reduction, the selectivity for Pd over Pt remained sufficiently high to support its preferential extraction. These findings underscore the importance of evaluating extractant performance not only in simplified single-metal systems but also under more representative multi-component conditions.

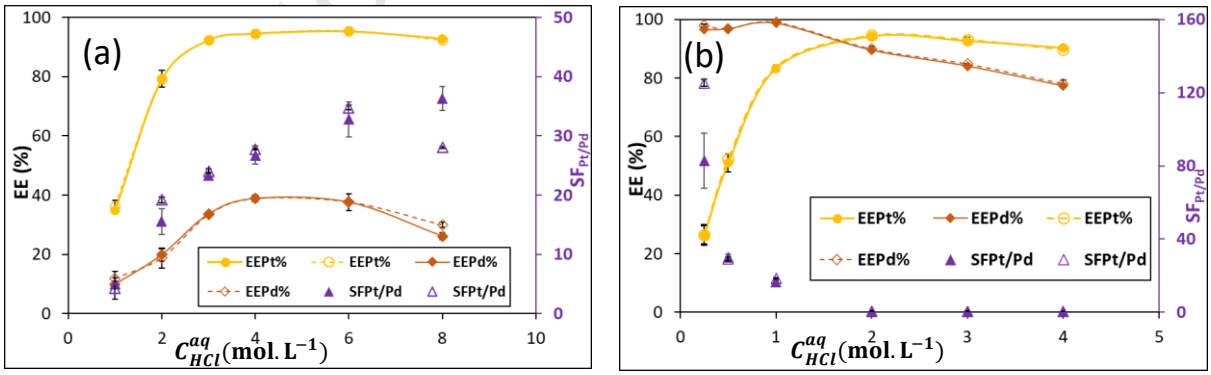

Fig. 10. Comparison of Pt(IV) and Pd(II) extraction from mono- and bimetallic solutions using (a) TOCA (x_{TOPO} = 0.40) and (b) LICA (x_{Lid} = 0.50). Conditions: $C_{Pt}^{aq} = 5$ mmol. L^{-1} ; $C_{Pd}^{aq} = 5$ mmol. L^{-1}; $S/F = 0.5$ (mL. mL^{-1}); $\omega = 900\ rpm$; $t = 5$ min; $T = 25\ °C$. Open symbols denote single-metal data; solid symbols indicate binary-metal data. Lines are visual guides. All data points in the figures are presented as mean values from three

independent experiments (n=3), with error bars denoting the standard deviation (±σ). Error bars are included for all data points; however, in some cases they are too small to be visually distinguished.

From the analysis of the different operating conditions for the extraction of Pt and Pd in single metal and binary metal solutions presented throughout Section 3.2, the values of the extraction performance indicators *EE*, *D* and *SF* achieved are comparable or improve in some cases those in previous works with DESs and other solvents as extractants, as shown in Tables S1a and S1b.

3.3. Extraction mechanism elucidation

The extraction behaviour of PGMs in DESs is primarily governed by the metal speciation in the aqueous phase and the intermolecular interactions between the extractant and metal complexes within the DES component network [29]. Accordingly, FT-IR and UV-visible spectroscopies were employed to clarify the extraction mechanisms of Pt(IV) and Pd(II) using TOCA and LICA.

Fig. 11(a) and 11(b) show the FT-IR spectra of TOCA before and after Pt(IV) extraction. The spectra revealed distinct changes in key functional groups involved in hydrogen bonding and metal coordination. The O–H stretching vibration of Carv, initially observed at 3161 cm^{-1} in fresh DES, shifted to 3198 cm^{-1} and became sharper after contact with the acidic Pt solution. This shift and band sharpening are consistent with a weakening and partial reorganisation of the hydrogen bond between the phenolic O–H and the phosphoryl oxygen of TOPO, implying partial disruption of the hydrogen-bonding network between TOPO and Carv in the Pt-loaded DES phase. Concurrently, the P=O stretching band of TOPO red shifted from 1139 to 1117 cm^{-1}, reflecting the protonation of the phosphoryl oxygen and formation of TOPO$\cdots\mathrm{H}^{+}$ adducts, as widely reported within the literature [34,35]. These protonated TOPO species are responsible for stabilising the $[\mathrm{PtCl}_6]^{2-}$complex through outer-sphere ion-pairing, maintaining charge neutrality and promoting solvation in the DES phase [33,68]. Overall, the FT-IR results support the mechanism in which Pt(IV) extraction with TOCA is facilitated by protonated TOPO, which act as the primary binding sites for $[\mathrm{PtCl}_6]^{2-}$. Simultaneously, acid co-extraction perturbs the internal hydrogen bonding between TOPO and Carv, causing a partial reorganisation of the TOCA structure.

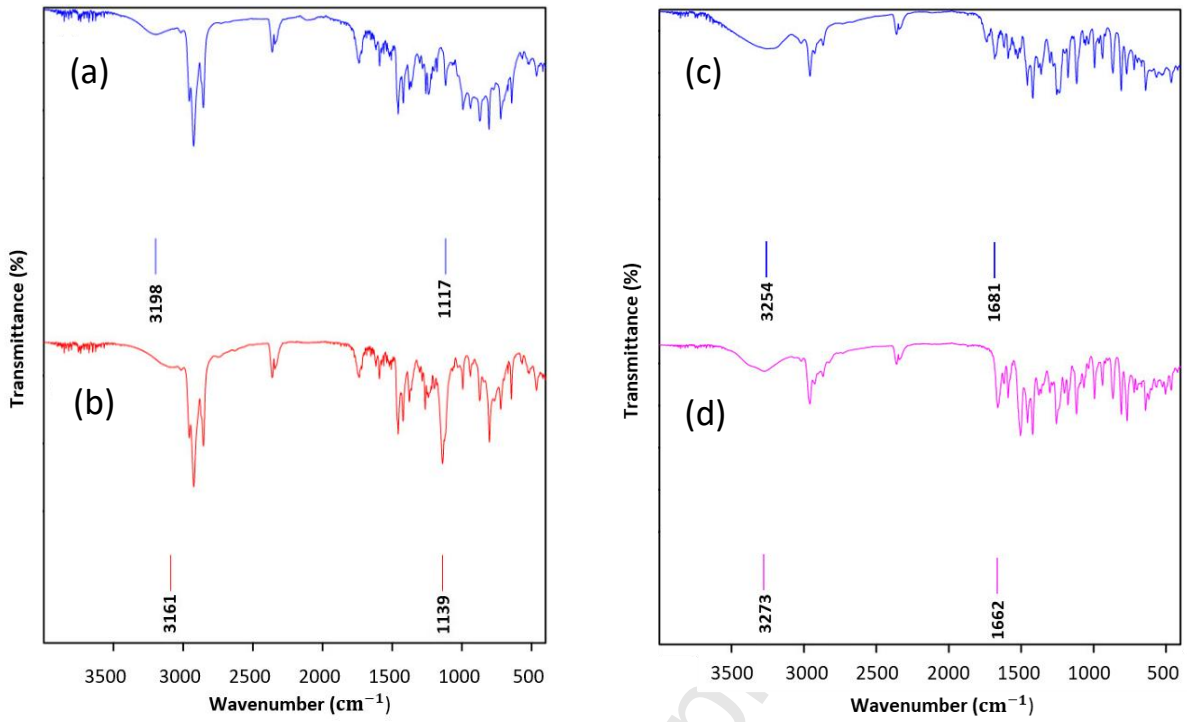

Fig. 11. FT-IR spectra of DESs before and after metal extraction from single-metal model solution (a) TOCA after Pt(IV) extraction, (b) fresh TOCA, (c) LICA after Pd(II) extraction, (d) fresh LICA.

The FT-IR spectra of LICA before and after Pd(II) extraction offers valuable insights into the molecular interactions underlying the Pd extraction process (Fig. 11(c) and 11(d)). In fresh LICA, characteristic bands appeared at 3273 cm^{-1} (amide N–H stretch) and 1662 cm^{-1} (amide C=O stretch). Following Pd extraction from aqueous solution, the N–H band shifted progressively to lower wavenumber (3254 cm^{-1}), suggesting protonation of the tertiary amine and disruption of potential intramolecular hydrogen bonding between amide N–H and lone pair on tertiary amine. Simultaneously, the C=O stretch shifted from 1662 to 1681 cm^{-1}, consistent with the electron-withdrawing effect of the protonated amine, which strengthens the C=O bond. These spectral changes strongly support that Pd(II) extraction proceeds via neutral ion-pair association between $[\mathrm{PdCl_4}]^{2-}$and the protonated tertiary amine ($R_3N\ldots H^+$) of Lid, confirming the key role of Lid as the active extracting component [36].

To examine metal speciation, the UV-visible spectra of Pt(IV) and Pd(II) in their respective initial acidic single-metal aqueous phases and the post-extraction DES phases were analysed. As illustrated in Fig. 12(a), Pt(IV) exhibits two characteristic absorption bands at ~205 nm and 262 nm, corresponding to the characteristic of $[\mathrm{PtCl_6}]^{2-}$ in chloride-rich acidic media [34,69,70]. After Pt(IV) extraction into TOCA ($\mathrm{x_{TOPO}}$ = 0.40), the phase displayed bands at ~205.5 nm and 275 nm. This spectral shift from 262 to 275 nm reflects the solvatochromic effects and coordination between $[\mathrm{PtCl_6}]^{2-}$and TOPO$\cdots H^+$, as also supported by FT-IR analysis, suggesting that Pt remained as $[\mathrm{PtCl_6}]^{2-}$ in TOCA phase [34,71]. Additionally, shoulders near 220 nm and 279.5 nm align with the known absorbance of free Carv [72],

suggesting the partial dissociation of Carv from the TOCA hydrogen-bond network, also evidenced by FT-IR.

For Pd(II) in $C_{HCl}^{aq} = 0.25\ \mathrm{mol.\,L^{-1}}$, absorption bands at ~223 nm and 280 nm confirmed $[PdCl_4]^{2-}$ speciation, as depicted in Fig. 12(b) [73,74]. Following Pd extraction into LICA ($x_{Lid} = 0.50$), the post-extraction DES showed relatively similar absorption features, with slight shifts to ~222 nm and 275.5 nm, indicating minor changes in the solvation environment, while Pd remained as $[PdCl_4]^{2-}$ during extraction into the LICA phase. A weak shoulder near ~279 nm, overlapping with the Pd(II) band, was also observed and attributed to unbound carvacrol, consistent with the partial disruption of LICA network and partial leaching of Lid molecules to the raffinate phase [72,75], as further revealed and discussed in Section 3.4.

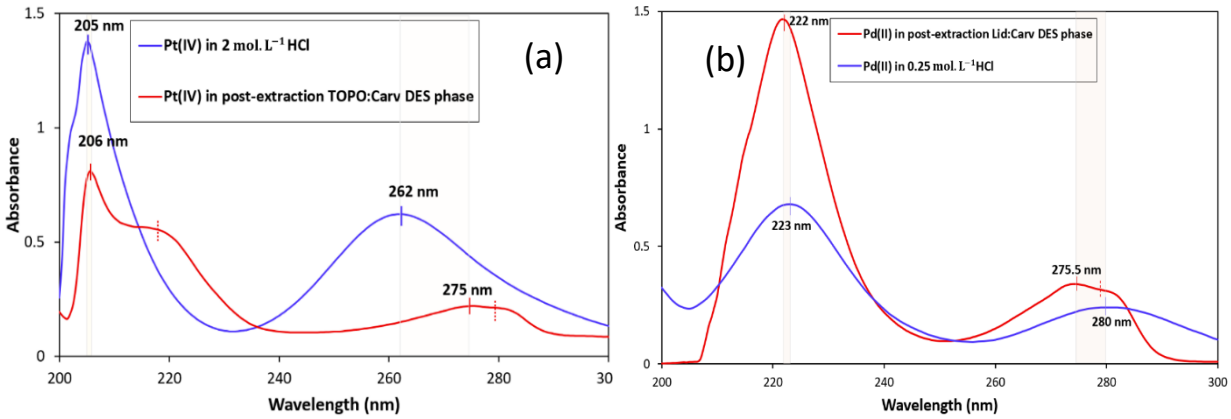

Fig. 12. UV-visible spectra of (a) Pt(IV) in $C_{HCl}^{aq} = 2\ \mathrm{mol.\,L^{-1}}$ (blue line) and in the post-extraction TOCA ($x_{TOPO} = 0.40$) phase (red line), (b) Pd(II) in $C_{HCl}^{aq} = 0.25\ \mathrm{mol.\,L^{-1}}$ (blue line) and in the post-extraction LICA ($x_{Lid} = 0.50$) phase (red line).

To further support the proposed proton-mediated extraction mechanism, the pH of the aqueous phase was measured before and after metal extraction. For Pt(IV) extraction from $C_{HCl}^{aq} = 2\ \mathrm{mol.\,L^{-1}}$ using TOCA, the pH increased from –0.3 to –0.1, while for Pd extraction from $C_{HCl}^{aq} = 0.25\ \mathrm{mol.\,L^{-1}}$ with LICA, the pH rose from 0.6 to 5.72. These notable increases in pH reflect a significant reduction in aqueous acidity, consistent with the co-extraction of protons into the DES phase.

Overall, the combined results from FT-IR, UV-visible, and pH measurements strongly support the proposed mechanism, in which Pt(IV) and Pd(II) extraction using TOCA and LICA proceeds via a neutral ion-pair association pathway, coupled with proton co-extraction, as depicted in Fig. 13. The co-extracted protons not only facilitate the electrostatic pairing with the negatively charged metal chloro-complexes, enabling their transfer into the DES phase, but also contribute to structural reorganisation within the DES network. It should also be noted that the location of chlorometalate-DES association, whether occurring at the aqueous-organic interface or within the bulk DES phase, remains unresolved.

Addressing this question would necessitate specialised microscopic and interface-sensitive techniques, such as tensiometry, X-ray reflectivity, or fluorescence-based methods, to directly probe interfacial adsorption and complexation phenomena [76].

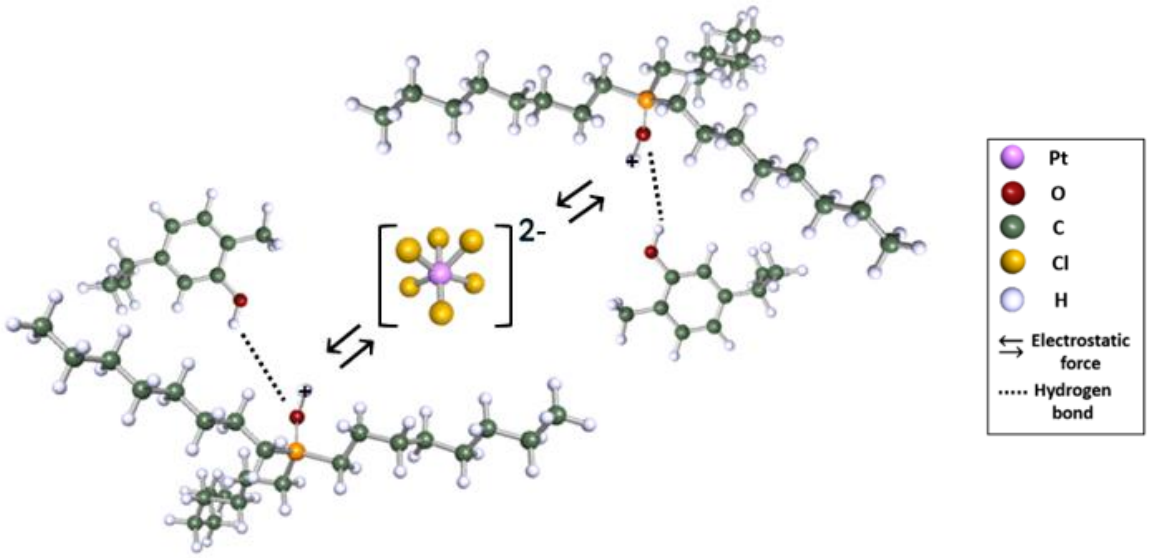

Fig. 13. Schematic illustrating the proposed neutral ion-pair association mechanism for $[PtCl_6]^{2-}$extraction using TOCA.

3.4. Pt and Pd back-extraction and DES Recycling

In view of the circularity of prospective SX processes, the regeneration of the DESs as the extracting phase is essential owing to economic and environmental sustainability considerations. This is approached here through back-extraction (stripping) of Pt(IV) and Pd(II) from the loaded DES phases.

Fig. 14(a) shows the stripping efficiency (SE) of Pt and Pd from post-extraction TOCA using various stripping reagents. Despite previous reports on effective PGM back-extraction using 0.2 $\mathrm{mol.\,L^{-1}}$ KSCN [36], it proved completely ineffective in this study, achieving only 6.62% Pt stripping and no detectable Pd removal. In contrast, water showed moderate stripping performance, recovering 88.27% of Pt and 65.27% of Pd. While this highlights its potential as a green stripping medium, incomplete metal recovery may limit its practical applicability in closed-loop systems. The use of 0.0005 $\mathrm{mol.\,L^{-1}}$ EDTA markedly improved stripping efficiency, with SE of both Pt and Pd exceeding 90%, attributed to the strong chelating nature of EDTA that promotes metal-ligand exchange [77]. Notably, nearly complete stripping of both metals was accomplished with 0.1 $\mathrm{mol.\,L^{-1}}$ thiourea in 0.5 $\mathrm{mol.\,L^{-1}}$ HCl, consistent with previous studies [32,62,78,79].

On the basis of the above results, EDTA and acidified thiourea were chosen for a series of successive extraction-striping tests to evaluate the long-term reusability of TOCA ($x_{TOPO} = 0.40$). As shown in Fig. 14(b), with acidified thiourea, Pd EE progressively increased over successive cycles, from 19.80% (fresh DES) to 27.93 % and 31.53 % after the first and second regenerations, respectively, and $SF_{Pt/Pd}$ decreased substantially. This trend suggests that thiourea was partially partitioned into the TOCA phase, leading to the formation of TOPO–thiourea eutectic-type adducts that enhanced Pd complexation and, consequently, diminished selectivity, consistent with a previous report on TOPO:N,N'-dihexylthiourea eutectic systems [78]. In contrast, EDTA-regenerated TOCA maintained constant EE and selectivity over five successive cycles (Fig. 14(c)), demonstrating operational robustness and suitability for long-term reuse.

To further confirm the chemical stability of TOCA, FT-IR spectra were recorded for the regenerated solvent after the first (R1_TOCA) and fourth (R4_TOCA) cycles (Fig. 14(d). No detectable band shifts or new bands were observed, suggesting that the molecular structure of the solvent remained intact despite repeated exposure to acidic and chelating environments. These results affirm that EDTA-regenerated TOCA is chemically stable, reusable, and maintains selectivity over multiple cycles. Accordingly, it constitutes a sustainable and industrially relevant extractant for the selective recovery of Pt(IV) over Pd(II) from real leachate.

Journal Pre-proof

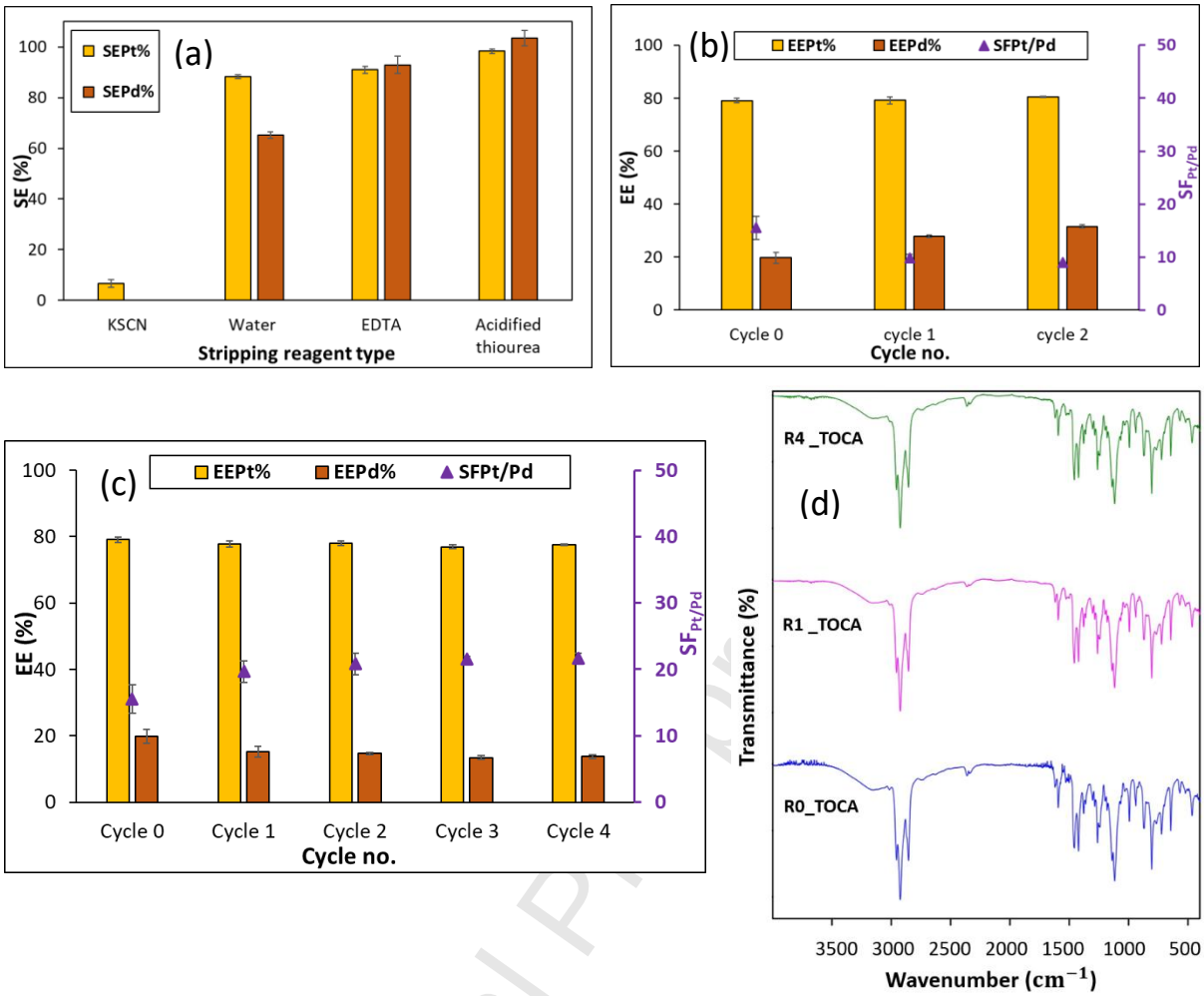

Fig. 14. (a) SE of Pt(IV) and Pd(II) from metal-loaded TOCA ($x_{TOPO} = 0.40$) using various stripping agents. Conditions: extract-to-strip volumetric phase ratio of 0.5 $mL.mL^{-1}$; $\omega = 900\ rpm$; $t = 60$ min; $T = 25\ °C$; (b, c) Evaluation of Pt(IV) and Pd(II) EE and $SF_{Pt/Pd}$ using TOCA ($x_{TOPO} = 0.40$) over successive extraction-stripping cycles under optimised extraction conditions: $C_{HCl}^{aq} = 2$ mol. L^{-1}; S/F = 0.5 (mL. mL^{-1}); $t = 5$ min; $T = 25\ °C$) using TOCA regenerated with (b) 0.1 mol. L^{-1} thiourea in 0.5 mol. L^{-1}HCl and (c) 0.0005 mol. L^{-1} EDTA; (d) FT-IR spectra of fresh and EDTA-regenerated TOCA after the first and fourth separation cycles. All data in figures (a)-(c) are presented as mean values from three independent experiments (n=3), with error bars denoting the standard deviation (±σ). Error bars are included for all data; however, in some cases they are too small to be visually distinguished.

Similarly, the back-extraction of Pd(II) and Pt(IV) from metal-loaded LICA ($x_{Lid} = 0.50$) was tested using those prepared stripping agents. Given that Pd extraction into the LICA phase was predominant, demonstrated by a high distribution ratio of 69.08 and EE of 96.55%, while Pt exhibited significantly lower extraction performance ($D_{Pt} = 0.82$; $EE_{Pt} = 25.74\%$), it was found that all stripping reagents, except 0.1 mol. L^{-1} thiourea in 0.5 mol. L^{-1} HCl, exhibited negligible effectiveness in Pd recovery (Fig. 15(a)). To evaluate the recyclability of regenerated LICA by acidified thiourea, multiple extraction-stripping cycles were performed. Notably, after the first regeneration and reuse, the LICA-rich extract

phase exhibited a distinct colour change to black (see Fig. 15(b)), suggesting that chemical reactions within the DES phase occurred. This observation aligns with previous reports on thiourea degradation in the presence of oxidising agents or even atmospheric oxygen, resulting in the formation of formamidine disulfide, a reactive intermediate known to trigger side reactions in the DES phase [80–82]. To mitigate such degradation and remove residual thiourea from the recycled LICA, a water-washing step was performed as a scrubbing process following the stripping stage, as previously recommended [29,83]. Experimental validation confirmed the effectiveness of this step, with no detectable signs of chemical degradation or side reactions, as depicted in Fig. 15(b). Consequently, a series of extraction-stripping-water washing cycles was conducted. As shown in Fig. 15(c), Pt EE sharply surged from 26.21% to 78.63% after the first cycle and reached near-complete extraction by the third cycle ($\mathrm{EE_{Pt}} = 99.85\%$), with a drastic decline in $\mathrm{SF_{Pd/Pt}}$, from 82.82 to 5.29.

Visual inspection revealed a gradual reduction in the volume of the LICA phase over consecutive extraction cycles (Table S4), indicating some leaching of the DES into the aqueous phase, calculated to be between 8.15% and 20.31% of LICA phase. This observation, together with previous reports of partial Lid leaching into the raffinate phase [75], suggests that the enhanced Pt extraction performance may stem from a shift in the HBA:HBD molar ratio, resulting in a lower Lid mole fraction in the regenerated LICA. This aligns with earlier findings on the impact of HBA:HBD molar ratios on Pt and Pd extraction performance using LICA systems (Section 3.2.1). To confirm the Lid loss, FT-IR characterisation was performed on aqueous Pd solutions before and after extraction with LICA ($\mathrm{x_{Lid}} = 0.50$). The spectra (Fig. 15(d)) displayed new peaks at 1547 and 1473 $\mathrm{cm^{-1}}$ in raffinate phase, corresponding to C–N and C=C stretching vibrations, respectively, thus confirming the partial migration of Lid into the aqueous phase. Such Lid leaching into the aqueous phase likely contributes to an increase in the pH value of the aqueous phase observed after Pd extraction with the LICA system compared with that seen for Pt extraction with TOCA. Therefore, an additional step to replenish the Lid lost during extraction is recommended to maintain a consistent DES molar composition, ensuring stable extraction performance and recyclability, both of which are critical for industrial-scale implementation.

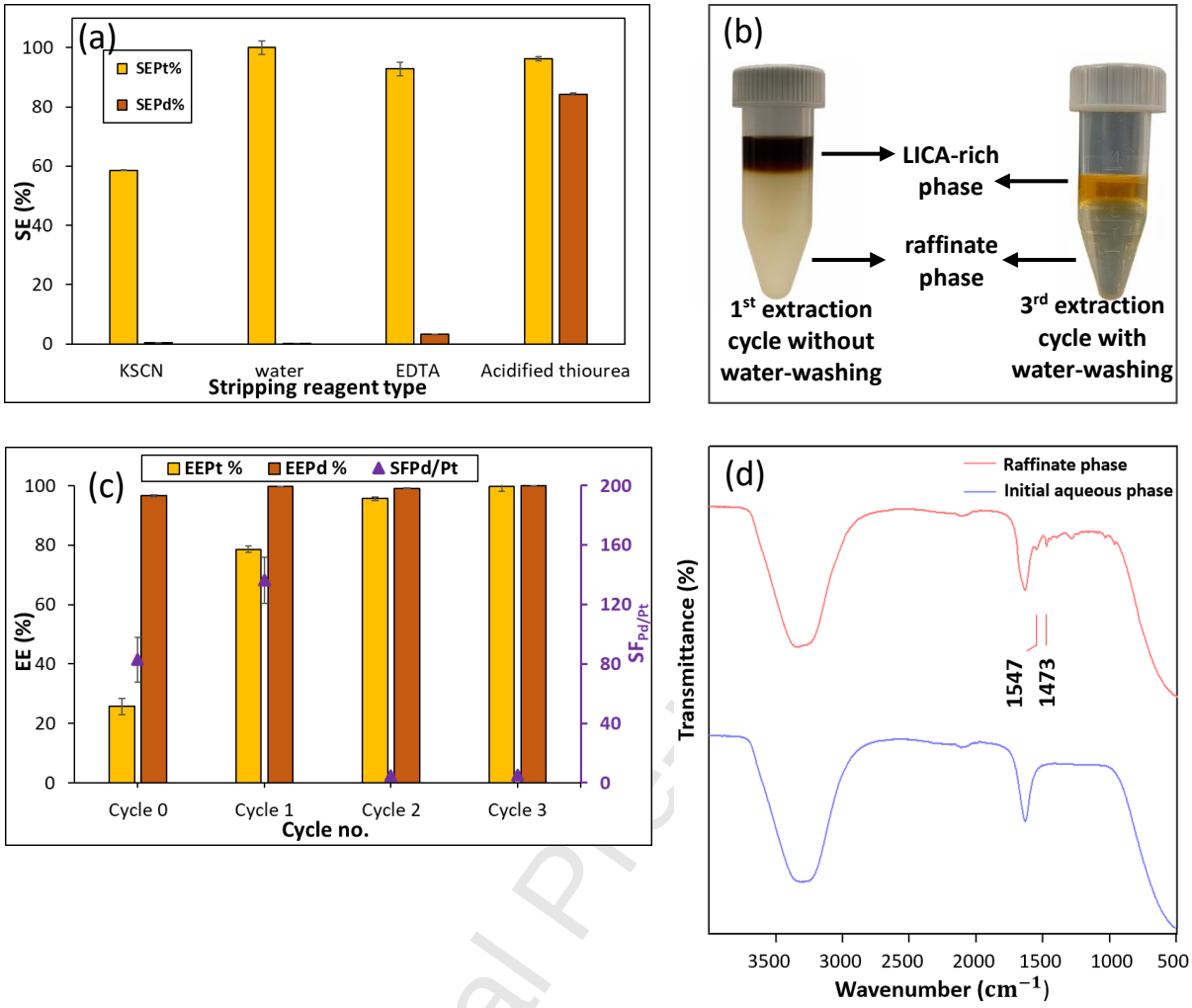

Fig. 15. (a) SE of Pt(IV) and Pd(II) from metal-loaded LICA ($x_{Lid} = 0.50$) using various stripping agents. Conditions: extract-to-strip volumetric phase ratio of 0.5 $mL.mL^{-1}$, $\omega = 900\ rpm$; $t = 60$ min; $T = 25\ °C$; (b) schematic visualisation of LICA degradation; (c) Evaluation of Pt(IV) and Pd(II) EE and $SF_{Pt/Pd}$ over successive extraction-stripping-water washing cycles using LICA ($x_{Lid} = 0.50$) regenerated with 0.1 $mol.L^{-1}$ thiourea in 0.5 $mol.L^{-1}$HCl under optimised extraction conditions: $C_{HCl}^{aq} = 0.25\ mol.L^{-1}$; $S/F = 0.5\ (mL.mL^{-1})$, $\omega = 900\ rpm; t = 5\ min; T = 25\ °C$; (d) FT-IR spectra of aqueous phase before and after Pd(II) extraction using LICA. All data in figures (a) and (c) are presented as mean values from three independent experiments (n=3), with error bars denoting the standard deviation (±σ). Error bars are included for all data; however, in some cases they are too small to be visually distinguished.

3.5. Comparative assessment of mass-based green metrics for Pt and Pd extraction using DESs

A comparative assessment using mass-based green metrics was conducted to evaluate the performance of the developed carvacrol-based DESs for the extraction of Pt and Pd. The results were benchmarked against previously reported DES-based systems for Pt and Pd recovery, with a focus on four mass-balance-based key green chemistry metrics: *PMI*, $E - factor$, *SI*, and *MP* (%), with the results summarised in Table 3 following the definitions in equations 6-11.

Table 3. Comparison of mass-based green metrics for Pt and Pd extraction using DESs.

DES	$PMI_{Pt,Pd}$	PMI_{Pt}	PMI_{Pd}	$E-factor$	SI	MP (%)	Ref.
TOCA (x_{TOPO}=0.40)	1678.2	1905.2	14082.2	0.716	512.9	0.060	this study
LICA (x_{Lid}=0.50)	1936.3	5762.0	2916.2	0.961	639.3	0.052	this study
TOPO:thymol (x_{TOPO}=0.40)	5756.9	5968.9	162073.2	1.362	1764.7	0.017	[33]
TOPO:decanoic acid (x_{TOPO}=0.40)	5676.1	7683.4	21726.5	1.350	1705.1	0.018	[35]
Lid:decanoic acid (x_{Lid}=0.50)	6297.4	9301.0	19501.1	0.859	202.7	0.016	[36]

PMI serves as a key indicator of material efficiency, representing the total mass of materials used per unit mass of recovered Pt and Pd [84]. Among the studied systems, TOCA and LICA DESs exhibited the lowest $PMI_{Pt,Pd}$ values at 1678.2 and 1936.3, respectively. These results suggest superior material efficiency for the carvacrol-based DES systems, particularly when compared to TOPO:thymol, TOPO:decanoic acid, and Lid:thymol solvents [33,35,36].

Notably, a system composed of Lid:decanoic acid (1:2) DES diluted in *n*-heptane has previously been reported as highly selective for Pd extraction, achieving EE of 100% for Pd and only 7.63% for Pt, with a notably low $PMI_{Pt,Pd}$ of 1445.7 [37]. However, due to the poor environmental profile of *n*-heptane, assigned an environmental hazard score of 7 according to the CHEM21 solvent selection guide [85], this system was excluded from the comparative greenness assessment.

To further assess solvent selectivity and its relevance to green metrics, *PMI* values were calculated separately for Pt and Pd. The TOCA system demonstrated the lowest PMI_{Pt} (1905.2), while the LICA system showed the lowest PMI_{Pd} (2916.2), aligning well with the selectivity trends observed in the LLX experiments.

The $E-factor$, which quantifies the amount of waste generated relative to the mass of Pt and Pd obtained as products from the separation, further supports the green credentials of the proposed systems. A lower $E-factor$ indicates a cleaner process. TOCA exhibited the lowest $E-factor$ at 0.716, while LICA and a previously reported Lid:thymol (1:1) system also achieved values below 1 (0.961 and 0.859, respectively), highlighting their environmentally favourable profiles [45,84].

SI is another commonly used green metric which quantifies the amount of solvent consumption per unit mass of recovered Pt and Pd. The Lid:thymol (1:1) system recorded the lowest *SI* at 202.7, which corresponds to its low *S/F* = 1:30 $(\mathrm{g.\,mL^{-1}})$ in LLX experiments. However, when an *S/F* of 0.5 $(\mathrm{mL.\,mL^{-1}})$ was applied for the consistency with the rest of extraction systems, the *SI* of the Lid:thymol system increased significantly to 1719.1 (approximately 8 times greater value). This suggests that TOCA and LICA systems exhibit relatively lower *SI* values at a fixed *S/F* of 0.5, with values of 512.9 and 639.3, respectively. Notably, the $E-factor$ of the Lid:thymol system was considerably improved at a *S/F* = 0.5, highlighting the significant influence of process conditions on green performance. *MP* was found to follow the same trend as $PMI_{Pt,Pd}$, further reinforcing the comparative advantages of TOCA and LICA.

Overall, the integrated assessment of *PMI*, $E-factor$, *SI*, and *MP* clearly indicates that the carvacrol-based DESs developed in this study, namely TOCA and LICA, show good green prospects for the selective extraction of Pt or Pd. Their lower material consumption, reduced waste generation, and improved solvent utilisation offer promising advantages over previously reported systems under similar experimental conditions.

4. Conclusions

In this study, novel non-ionic DESs comprising TOPO and Lid as HBAs and Carv as the HBD (TOCA and LICA, respectively) were designed for the selective separation of Pt and Pd. This design comprised of SLE curve predictions using COSMO-RS with experimental validation through DSC and visual measurements. The formation of hydrogen bonds was confirmed by FT-IR spectroscopy, corroborating the DES nature of LICA and TOCA.

Separation studies of Pt and Pd using TOCA and LICA identified optimum operational conditions, with HBA:HBD ratio (TOCA at $\mathrm{x_{TOPO}} = 0.40$ and LICA at $\mathrm{x_{Lid}} = 0.50$) and the aqueous HCl concentration ($C_{HCl}^{aq} = 2\ \mathrm{mol.\,L^{-1}}$ and $C_{HCl}^{aq} = 0.25\ \mathrm{mol.\,L^{-1}}$ for extractions with TOCA and LICA, respectively) being determinant. TOCA displayed a strong preference for Pt extraction, whereas LICA favoured Pd extraction. It was observed that there is a correlation between the composition of the DES relative to its proximity to its eutectic point and the extraction efficiency of Pt and Pd. As such, the greater the hydrogen bond interaction within the DES at hand, the lower the ability to extract metals from the aqueous solutions. This highlights a critical trade-off between structural stability and functional flexibility in DES performance.

The extraction behaviour of Pt and Pd is strongly governed by the interplay between acidity, metal speciation, and chloride activity. While moderate HCl concentration promotes extraction by stabilising

anionic chlorometalate species and enabling proton-assisted coordination within the DES phase, excessive HCl concentration introduce competitive effects between $Cl^-$and anionic PGM-chloro complexes that hinder metal–extractant interactions. This effect was more pronounced for $[PdCl_4]^{2-}$, which is more susceptible to hydrolysis and chloride competition than the more stable $[PtCl_6]^{2-}$.

Supported by FT-IR, UV-visible, and pH measurements, the extraction was proposed to proceed via a neutral ion-pairing association mechanism, mediated by the co-extraction of protons, leading to the formation of HBA…H^+ adducts that serve as counter-ions for the anionic PGM-chloro complexes. In terms of thermodynamics, extraction with TOCA is exothermic for both metals, with the process being spontaneous for Pt but non-spontaneous for Pd. In contrast, the use of LICA showed exothermic and spontaneous behaviour for Pd extraction, but endothermic and non-spontaneous for Pt.

Pt and Pd back-extraction and DES regeneration could be achieved using 0.0005 $mol.L^{-1}$ EDTA from metal-loaded TOCA, and 0.1 $mol.L^{-1}$ thiourea in 0.5 $mol.L^{-1}$ HCl from metal-loaded LICA. TOCA (x_{TOPO} = 0.40) exhibited excellent recyclability, maintaining consistent extraction performance and Pt selectivity over five extraction–stripping cycles with no significant change in structure or performance attaining $EE_{Pt} = 79.07\%$ with the fresh solvent and $EE_{Pt} = 77.53\%$ after the fourth recycle. LICA (x_{Lid} = 0.50) retained high Pd extraction efficiency ($EE_{Pd} = 99.97\%$ at the third cycle); however, its selectivity for Pd over Pt declined over successive cycles, with the $SF_{Pd/Pt}$ decreasing from 82.82 (fresh LICA) to 5.29 after three cycles. This loss of selectivity was attributed to Lid leaching into the aqueous phase. To mitigate this, incorporating a make-up stream prior to reuse is recommended to restore the 1:1 HBA:HBD composition of the DES LICA, thereby sustaining both extraction efficiency and selectivity.

Finally, an assessment considering mass-based green metrics showed very promising results for the use of these carvacrol-based DESs for the separation of Pt and Pd, particularly in terms of E-factor (<1), reduced process mass intensity and high mass productivity compared to previous efforts.

Overall, the promising outcomes from both mono- and bimetallic model systems highlight the significant potential of TOCA and LICA as environmentally benign, tunable media for the efficient and selective LLX of Pt and Pd, respectively.

CRediT authorship contribution statement

Sahar Gholami: Conceptualisation, Methodology, Software, Formal analysis, Investigation, Data Curation, Writing - Original Draft, Writing - Review & Editing, Visualisation.

Pablo López-Porfiri: Methodology, Validation, Writing - Review & Editing.

María Pérez-Page: Methodology, Resources, Writing – review & editing, Supervision, Project administration, Funding acquisition.

Jesús Esteban: Conceptualisation, Methodology, Validation, Resources, Writing - Original Draft, Writing - Review & Editing, Supervision, Project administration, Funding acquisition.

Conflict of interest

There are no conflicts of interest to declare.

Data availability

Data will be made available on request. Supplementary information is available, including SLE theoretical background and workflow of DFT calculations and COSMO-RS prediction, characterisation methodology and results (DSC, FT-IR, ICP-OES, UV-visible), mass transfer limitations assessment in LLX, additional information for the thermodynamic assessment of metal LLX, and analysis of LICA leaching into the aqueous phase based on volume change.

Acknowledgments

The University of Manchester is acknowledged for funding of a PGRTA PhD scholarship for SG. JE acknowledges grant RYC2022-035654-I funded by MICIU/AEI/10.13039/501100011033 and by ESF+ and grant PID2024-156902OA-I00 funded by MICIU/AEI/10.13039/501100011033 and ERDF/EU. PLP and MPP acknowledge grants EPSRC EP/V047078/1 and EP/W03395X/1. JE and MPP also acknowledge funding from the British Council through the Springboard Programme for UK-Spain partnerships (project GRACE). The authors gratefully acknowledge the valuable contributions of Jamie Tibble-Howlings, Shahla Khan, and Otis Leahair from the Analytical Laboratory, Department of Chemical Engineering, University of Manchester, for their support and assistance with characterisation measurements.

References

[1] V.T. Nguyen, S. Riaño, E. Aktan, C. Deferm, J. Fransaer, K. Binnemans, Solvometallurgical Recovery of Platinum Group Metals from Spent Automotive Catalysts, ACS Sustain. Chem. Eng. 9 (2021) 337–350. https://doi.org/10.1021/acssuschemeng.0c07355.

[2] S. Ilyas, R.R. Srivastava, H. Kim, H.A. Cheema, Hydrometallurgical recycling of palladium and platinum from exhausted diesel oxidation catalysts, Sep. Purif. Technol. 248 (2020) 117029. https://doi.org/10.1016/j.seppur.2020.117029.

[3] S. Papagianni, A.-M. Moschovi, E. Polyzou, I. Yakoumis, Platinum Recovered from Automotive Heavy-Duty Diesel Engine Exhaust Systems in Hydrometallurgical Operation, Metals (Basel). 12

(2021) 31. https://doi.org/10.3390/met12010031.

[4] W. Mabhulusa, K.E. Sekhosana, X. Fuku, The impact and performance of carbon-supported platinum group metal electrocatalysts for fuel cells, Int. J. Electrochem. Sci. 19 (2024) 100524. https://doi.org/10.1016/j.ijoes.2024.100524.

[5] D. Guo, Q. Pan, Y. Gao, Platinum compounds constructing interface structure strategies for electrolysis hydrogen production, Chem. Commun. 61 (2025) 7543–7562. https://doi.org/10.1039/D5CC01094B.

[6] B.K. Woodward, Platinum group metals (PGMs) for permanent implantable electronic devices, in: Precious Met. Biomed. Appl., Elsevier, 2014: pp. 130–147. https://doi.org/10.1533/9780857099051.2.130.

[7] A. Seretis, P. Diamantopoulou, I. Thanou, P. Tzevelekidis, C. Fakas, P. Lilas, G. Papadogianakis, Recent advances in ruthenium-catalyzed hydrogenation reactions of renewable biomass-derived levulinic acid in aqueous media, Front. Chem. 8 (2020) 1–22. https://doi.org/10.3389/fchem.2020.00221.

[8] A.E. Hughes, N. Haque, S.A. Northey, S. Giddey, Platinum group metals: A review of resources, production and usage with a focus on catalysts, Resources 10 (2021) 1–40. https://doi.org/10.3390/resources10090093.

[9] G.M. Mudd, S.M. Jowitt, T.T. Werner, Global platinum group element resources, reserves and mining – A critical assessment, Sci. Total Environ. 622–623 (2018) 614–625. https://doi.org/10.1016/j.scitotenv.2017.11.350.

[10] European Commission, Study on the EU's list of critical raw materials, 2020. https://doi.org/10.2873/587825.

[11] J. Zhang, M.P. Everson, T.J. Wallington, F.R. Field, R. Roth, R.E. Kirchain, Assessing economic modulation of future critical materials use: The case of automotive-related platinum group metals, Environ. Sci. Technol. 50 (2016) 7687–7695. https://doi.org/10.1021/acs.est.5b04654.

[12] Gold.DE, Platinum bars, (n.d.). https://www.gold.de/kaufen/platin/platinbarren/ (accessed August 29, 2025).

[13] GOLDE.DE, Compare palladium bar prices, (n.d.). https://www.gold.de/kaufen/palladium/palladiumbarren/ (accessed August 29, 2025).

[14] A. Balali, S. Gholami, M. Javanmardi, A. Valipour, A. Yunusa-Kaltungo, Assessment of heavy metal pollution in the soil of a construction and demolition waste landfill, Environ. Nanotechnology, Monit. Manag. 20 (2023) 100856. https://doi.org/10.1016/j.enmm.2023.100856.

[15] Z. Yuan, H. Liu, W.F. Yong, Q. She, J. Esteban, Status and advances of deep eutectic solvents for

metal separation and recovery, Green Chem. 24 (2022) 1895–1929. https://doi.org/10.1039/D1GC03851F.

[16] I. Chidunchi, M. Kulikov, R. Safarov, E. Kopishev, Extraction of platinum group metals from catalytic converters, Heliyon 10 (2024) e25283. https://doi.org/10.1016/j.heliyon.2024.e25283.

[17] K. Pianowska, J. Kluczka, G. Benke, K. Goc, J. Malarz, M. Ochmański, K. Leszczyńska-Sejda, Solvent extraction as a method of recovery and separation of platinum group metals, Materials (Basel). 16 (2023) 4681. https://doi.org/10.3390/ma16134681.

[18] S. Karim, Y. Ting, Recycling pathways for platinum group metals from spent automotive catalyst: A review on conventional approaches and bio-processes, Resour. Conserv. Recycl. 170 (2021) 105588. https://doi.org/10.1016/j.resconrec.2021.105588.

[19] K. Binnemans, P.T. Jones, Solvometallurgy: An emerging branch of extractive metallurgy, J. Sustain. Metall. 3 (2017) 570–600. https://doi.org/10.1007/s40831-017-0128-2.

[20] R. Nithya, C. Sivasankari, A. Thirunavukkarasu, A. Silver, Electronic waste generation, regulation and metal recovery: a review, Environ. Chem. Lett. 19 (2021) 1347–1368. https://doi.org/10.1007/s10311-020-01111-9.

[21] W. Zhuang, J.P. Fitts, C.M. Ajo-franklin, S. Maes, L. Alvarez-cohen, T. Hennebel, Recovery of critical metals using biometallurgy, Curr. Opin. Biotechnol. 33 (2015) 327–335. https://doi.org/10.1016/j.copbio.2015.03.019.

[22] M.K. Jha, J.C. Lee, M.S. Kim, J. Jeong, B.S. Kim, V. Kumar, Hydrometallurgical recovery/recycling of platinum by the leaching of spent catalysts: A review, Hydrometallurgy 133 (2012) 23–32. https://doi.org/10.1016/j.hydromet.2012.11.012.

[23] K. Alfonsi, J. Colberg, P.J. Dunn, T. Fevig, S. Jennings, T.A. Johnson, H.P. Kleine, C. Knight, M.A. Nagy, D.A. Perry, M. Stefaniak, Green chemistry tools to influence a medicinal chemistry and research chemistry based organisation, Green Chem. 10 (2008) 31–36. https://doi.org/10.1039/b711717e.

[24] N. Rodriguez Rodriguez, L. Machiels, K. Binnemans, p-Toluenesulfonic Acid-Based Deep-Eutectic Solvents for Solubilizing Metal Oxides, ACS Sustain. Chem. Eng. 7 (2019) 3940–3948. https://doi.org/10.1021/acssuschemeng.8b05072.

[25] D. Liu, B. Zhang, Y. Luo, P. Cui, X. Li, F. Zheng, G. Li, Y. Wang, Efficient stepwise separation of heavy metals from wastewater with hydrophobic deep eutectic solvents, Sep. Purif. Technol. 388 (2026) 136810. https://doi.org/10.1016/j.seppur.2026.136810.

[26] S. Gholami, A. Roosta, Bubble point of aqueous mixtures of sugar-based deep eutectic solvents and their individual components: Experimental study and modeling, J. Mol. Liq. 296 (2019)

111876. https://doi.org/10.1016/j.molliq.2019.111876.

[27] S. Gholami, A. Roosta, Experimental study and modeling of bubble point of aqueous mixtures of deep eutectic solvents based on dicarboxylic acids and choline chloride, J. Chem. Eng. Data 65 (2020) 2743–2750. https://doi.org/10.1021/acs.jced.0c00070.

[28] N. Schaeffer, I.C.M. Vaz, M.S. Pinheiro, F. Olea, T. Hanada, S. Dourdain, J.A.P. Coutinho, Examining the potential of type V DESs for the solvent extraction of metal ions, Green Chem. 27 (2025) 4438–4463. https://doi.org/10.1039/d5gc00489f.

[29] S. Gholami, M. Pérez-Page, C. D'Agostino, J. Esteban, (Deep) eutectic solvents for the separation of platinum group metals and rare earth elements: Characteristics, extraction mechanisms and state of the art, Chem. Eng. J. 505 (2025) 159497. https://doi.org/10.1016/j.cej.2025.159497.

[30] G. Shakiba, R. Saneie, H. Abdollahi, E. Ebrahimi, A. Rezaei, M. Mohammadkhani, Application of deep eutectic solvents (DESs) as a green lixiviant for extraction of rare earth elements from caustic-treated monazite concentrate, J. Environ. Chem. Eng. 11 (2023) 110777. https://doi.org/10.1016/j.jece.2023.110777.

[31] N. Tang, L. Liu, C. Yin, G. Zhu, Q. Huang, J. Dong, X. Yang, S. Wang, Environmentally benign hydrophobic deep eutectic solvents for palladium(II) extraction from hydrochloric acid solution, J. Taiwan Inst. Chem. Eng. 121 (2021) 92–100. https://doi.org/10.1016/j.jtice.2021.04.010.

[32] O. Mokhodoeva, V. Maksimova, A. Shishov, V. Shkinev, Separation of platinum group metals using deep eutectic solvents based on quaternary ammonium salts, Sep. Purif. Technol. 305 (2023) 122427. https://doi.org/10.1016/j.seppur.2022.122427.

[33] N. Schaeffer, J.H.F. Conceição, M.A.R. Martins, M.C. Neves, G. Pérez-Sánchez, J.R.B. Gomes, N. Papaiconomou, J.A.P. Coutinho, Non-ionic hydrophobic eutectics – versatile solvents for tailored metal separation and valorisation, Green Chem. 22 (2020) 2810–2820. https://doi.org/10.1039/D0GC00793E.

[34] R. Liu, Y. Geng, Z. Tian, N. Wang, M. Wang, G. Zhang, Y. Yang, Extraction of platinum(IV) by hydrophobic deep eutectic solvents based on trioctylphosphine oxide, Hydrometallurgy 199 (2021) 105521. https://doi.org/10.1016/j.hydromet.2020.105521.

[35] S.J.R. Vargas, G. Pérez-Sánchez, N. Schaeffer, J.A.P. Coutinho, Solvent extraction in extended hydrogen bonded fluids – separation of Pt(IV) from Pd(II) using TOPO- based type V DES, Green Chem. 23 (2021) 4540–4550. https://doi.org/10.1039/D1GC00829C.

[36] R. Liu, J. Hao, Y. Wang, Y. Meng, Y. Yang, A separation strategy of Au(III), Pd(II) and Pt(IV) based on hydrophobic deep eutectic solvent from hydrochloric acid media, J. Mol. Liq. 365 (2022)

120200. https://doi.org/10.1016/j.molliq.2022.120200.

[37] P.D. Ola, M. Matsumoto, Extraction of Au(III), Pt(IV), and Pd(II) from aqueous media with deep eutectic solvent dissolved in n-heptane as extractant, Indones. J. Chem. 23 (2023) 1735–1741. https://doi.org/10.22146/ijc.80862.

[38] A. Klamt, Conductor-like screening model for real solvents: A new approach to the quantitative calculation of solvation phenomena, J. Phys. Chem. 99 (1995) 2224–2235. https://doi.org/10.1021/j100007a062.

[39] D.O. Abranches, M.A.R. Martins, L.P. Silva, N. Schaeffer, S.P. Pinho, J.A.P. Coutinho, Phenolic hydrogen bond donors in the formation of non-ionic deep eutectic solvents: The quest for type V DES, Chem. Commun. 55 (2019) 10253–10256. https://doi.org/10.1039/c9cc04846d.

[40] T. Zhou, L. Chen, Y. Ye, L. Chen, Z. Qi, H. Freund, K. Sundmacher, An overview of mutual solubility of ionic liquids and water predicted by COSMO-RS, Ind. Eng. Chem. Res. 51 (2012) 6256–6264. https://doi.org/10.1021/ie202719z.

[41] J.P. Wojeicchowski, A.M. Ferreira, D.O. Abranches, M.R. Mafra, J.A.P. Coutinho, Using COSMO-RS in the Design of Deep Eutectic Solvents for the Extraction of Antioxidants from Rosemary, ACS Sustain. Chem. Eng. 8 (2020) 12132–12141. https://doi.org/10.1021/acssuschemeng.0c03553.

[42] Z. Song, J. Wang, K. Sundmacher, Evaluation of COSMO-RS for solid–liquid equilibria prediction of binary eutectic solvent systems, Green Energy Environ. 6 (2021) 371–379. https://doi.org/10.1016/j.gee.2020.11.020.

[43] E.L. Byrne, R. O'Donnell, M. Gilmore, N. Artioli, J.D. Holbrey, M. Swadźba-Kwaśny, Hydrophobic functional liquids based on trioctylphosphine oxide (TOPO) and carboxylic acids, Phys. Chem. Chem. Phys. 22 (2020) 24744–24763. https://doi.org/10.1039/d0cp02605k.

[44] M. Gras, L. Duclos, N. Schaeffer, V. Mogilireddy, L. Svecova, E. Chaînet, I. Billard, N. Papaiconomou, A comparison of cobalt and platinum extraction in hydrophobic and hydrophilic ionic liquids: Implication for proton exchange membrane fuel cell recycling, ACS Sustain. Chem. Eng. 8 (2020) 15865–15874. https://doi.org/10.1021/acssuschemeng.0c04263.

[45] R.A. Sheldon, Metrics of green chemistry and sustainability: Past, present, and future, ACS Sustain. Chem. Eng. 6 (2018) 32–48. https://doi.org/10.1021/acssuschemeng.7b03505.

[46] M.A.R. Martins, S.P. Pinho, J.A.P. Coutinho, Insights into the nature of eutectic and deep eutectic mixtures, J. Solution Chem. 48 (2019) 962–982. https://doi.org/10.1007/s10953-018-0793-1.

[47] P. López-Porfiri, P. Gorgojo, M. Gonzalez-Miquel, Green Solvent Selection Guide for Biobased Organic Acid Recovery, ACS Sustain. Chem. Eng. 8 (2020) 8958–8969.

https://doi.org/10.1021/acssuschemeng.0c01456.

[48] D.O. Abranches, J.A.P. Coutinho, Type V deep eutectic solvents: Design and applications, Curr. Opin. Green Sustain. Chem. 35 (2022) 100612. https://doi.org/10.1016/j.cogsc.2022.100612.

[49] D.O. Abranches, J.A.P. Coutinho, Everything you wanted to know about deep eutectic solvents but were afraid to be told, Annu. Rev. Chem. Biomol. Eng. 14 (2023) 141–163. https://doi.org/10.1146/annurev-chembioeng-101121-085323.

[50] A. Alhadid, L. Mokrushina, M. Minceva, Formation of glassy phases and polymorphism in deep eutectic solvents, J. Mol. Liq. 314 (2020) 113667. https://doi.org/10.1016/j.molliq.2020.113667.

[51] J.S. Chickos, G. Nichols, P. Ruelle, The Estimation of Melting Points and Fusion Enthalpies Using Experimental Solubilities, Estimated Total Phase Change Entropies, and Mobile Order and Disorder Theory, J. Chem. Inf. Comput. Sci. 42 (2002) 368–374. https://doi.org/10.1021/ci010341b.

[52] E.M. Barral, J.F. Johnson, Differential scanning calorimetry theory and applications, Tech. Methods Polym. Eval. Therm. Charact. Tech. (1970) 1–40.

[53] M. Bertuola, N. Fagali, M. Fernández Lorenzo de Mele, Detection of carvacrol in essential oils by electrochemical polymerization, Heliyon 6 (2020) e03714. https://doi.org/10.1016/j.heliyon.2020.e03714.

[54] N. Rajendiran, T. Mohandoss, J. Saravanan, Guest:host interactions of lidocaine and prilocaine with natural cyclodextrins: Spectral and molecular modeling studies, Spectrochim. Acta Part A Mol. Biomol. Spectrosc. 132 (2014) 387–396. https://doi.org/10.1016/j.saa.2014.04.123.

[55] R.G. Pearson, Hard and Soft Acids and Bases, J. Am. Chem. Soc. 85 (1963) 3533–3539. https://doi.org/10.1021/ja00905a001.

[56] R.G. Pearson, Hard and soft acids and bases, HSAB, part I: Fundamental principles, J. Chem. Educ. 45 (1968) 581–587.

[57] Y. Su, A Quantum Chemical Study of Environmental Catalysis at the Metal- Ceria Interface, Edinhoven University of Technology, 2019.

[58] V.T. Nguyen, J. Lee, M. Kim, S. Kim, A. Chagnes, G. Cote, Sustainable extraction and separation of precious metals from hydrochloric media using novel ionic liquid-in-water microemulsion, Hydrometallurgy 171 (2017) 344–354. https://doi.org/10.1016/j.hydromet.2017.06.003.

[59] C.S. Kedari, T. Coll, A. Fortuny, A. Sastre, Third Phase Formation in the Solvent Extraction System Ir(IV)—Cyanex 923, Solvent Extr. Ion Exch. 23 (2005) 545–559. https://doi.org/10.1081/SEI-200068505.

[60] U.G. Favero, N. Schaeffer, H. Passos, K.A.M.L. Cruz, D. Ananias, S. Dourdain, M.C. Hespanhol,

Solvent extraction in non-ideal eutectic solvents – Application towards lanthanide separation, Sep. Purif. Technol. 314 (2023) 123592. https://doi.org/10.1016/j.seppur.2023.123592.

[61] H.B. Trinh, S. Kim, T. Son, J. Lee, Platinum recycling from fuel cell-spent electrocatalysts using oxidative leaching in HCl solution, Clean. Eng. Technol. 18 (2024) 100709. https://doi.org/10.1016/j.clet.2023.100709.

[62] V.T. Nguyen, J. Lee, A. Chagnes, M. Kim, J. Jeong, G. Cote, Highly selective separation of individual platinum group metals (Pd, Pt, Rh) from acidic chloride media using phosphonium-based ionic liquid in aromatic diluent, RSC Adv. 6 (2016) 62717–62728. https://doi.org/10.1039/C6RA09328K.

[63] K. Abdi, M. Ezoddin, N. Pirooznia, Temperature-controlled liquid–liquid microextraction using a biocompatible hydrophobic deep eutectic solvent for microextraction of palladium from catalytic converter and road dust samples prior to ETAAS determination, Microchem. J. 157 (2020) 104999. https://doi.org/10.1016/j.microc.2020.104999.

[64] J. Lee, K. Kurniawan, S. Kim, V.T. Nguyen, B.D. Pandey, Ionic liquids-assisted solvent extraction of precious metals from chloride solutions, Sep. Purif. Rev. 52 (2023) 242–261. https://doi.org/10.1080/15422119.2022.2091458.

[65] J. YANG, F. KUBOTA, Y. BABA, N. KAMIYA, M. GOTO, Separation of precious metals by using undiluted ionic liquids, Solvent Extr. Res. Dev. Japan 21 (2014) 89–94. https://doi.org/10.15261/serdj.21.89.

[66] P. Anastas, J. Warner, Green chemistry: theory and practice, Oxford University Press, 2000. https://doi.org/10.1093/oso/9780198506980.001.0001.

[67] U. Otgonbayar, L. Sandig-Predzymirska, A. Thiere, A. Charitos, Solvent extraction of Pt, Ru, and Ir using Cyanex 923 in chloride media to develop a recycling route for spent polymer electrolyte membrane (PEM) electrolyzers, Hydrometallurgy 226 (2024) 106303. https://doi.org/10.1016/j.hydromet.2024.106303.

[68] J. Rydberg, Solvent Extraction Principles and Practice, Revised and Expanded, CRC Press, 2004. https://doi.org/10.1201/9780203021460.

[69] Y. Ueda, S. Morisada, H. Kawakita, M. Wenzel, J.J. Weigand, K. Ohto, Effective extraction of Pt(IV) as [PtCl6]2− from hydrochloric acid using a simple urea extractant, Sep. Purif. Technol. 277 (2021) 119456. https://doi.org/10.1016/j.seppur.2021.119456.

[70] M. Georgieva, B. Andonovski, Determination of platinum(IV) by UV spectrophotometry, Anal. Bioanal. Chem. 375 (2003) 836–839. https://doi.org/10.1007/s00216-003-1783-7.

[71] K. Anandhan, M. Cerón, V. Perumal, P. Ceballos, P. Gordillo-Guerra, E. Pérez-Gutiérrez, A.E. Castillo, S. Thamotharan, M.J. Percino, Solvatochromism and pH effect on the emission of a

triphenylimidazole-phenylacrylonitrile derivative: experimental and DFT studies, RSC Adv. 9 (2019) 12085–12096. https://doi.org/10.1039/C9RA01275C.

[72] C.G. Sokolik, J.-P. Lellouche, Hybrid-silica nanoparticles as a delivery system of the natural biocide carvacrol, RSC Adv. 8 (2018) 36712–36721. https://doi.org/10.1039/C8RA05898A.

[73] M. Shao, S. Li, C. Jin, M. Chen, Z. Huang, Recovery of Pd(II) from hydrochloric acid medium by solvent extraction–direct electrodeposition using hydrophilic/hydrophobic ILs, ACS Omega 5 (2020) 27188–27196. https://doi.org/10.1021/acsomega.0c03255.

[74] J.-F. Boily, T.M. Seward, Palladium(II) chloride complexation: Spectrophotometric investigation in aqueous solutions from 5 to 125°C and theoretical insight into Pd-Cl and Pd-OH2 interactions, Geochim. Cosmochim. Acta 69 (2005) 3773–3789. https://doi.org/10.1016/j.gca.2005.03.015.

[75] D.J.G.P. van Osch, D. Parmentier, C.H.J.T. Dietz, A. van den Bruinhorst, R. Tuinier, M.C. Kroon, Removal of alkali and transition metal ions from water with hydrophobic deep eutectic solvents, Chem. Commun. 52 (2016) 11987–11990. https://doi.org/10.1039/C6CC06105B.

[76] P. Sun, E.A. Binter, Z. Liang, M.A. Brown, A. V Gelis, I. Benjamin, M.K. Bera, B. Lin, W. Bu, M.L. Schlossman, Antagonistic role of aqueous complexation in the solvent extraction and separation of rare earth ions, ACS Cent. Sci. 7 (2021) 1908−1918. https://doi.org/10.1021/acscentsci.1c00960.

[77] S. Khare, A. Singhal, S. Rallapalli, A. Mishra, Bio-chelate assisted leaching for enhanced heavy metal remediation in municipal solid waste compost, Sci. Rep. 14 (2024) 14238. https://doi.org/10.1038/s41598-024-65280-1.

[78] A. van den Bruinhorst, S. Raes, S.A. Maesara, M.C. Kroon, A.C.C. Esteves, J. Meuldijk, Hydrophobic eutectic mixtures as volatile fatty acid extractants, Sep. Purif. Technol. 216 (2019) 147–157. https://doi.org/10.1016/j.seppur.2018.12.087.

[79] S. Ilyas, H. Kim, Recovery of Platinum-Group Metals from an Unconventional Source of Catalytic Converter Using Pressure Cyanide Leaching and Ionic Liquid Extraction, JOM 74 (2022) 1020–1026. https://doi.org/10.1007/s11837-021-05119-6.

[80] T. Groenewald, The dissolution of gold in acidic solutions of thiourea, Hydrometallurgy 1 (1976) 277–290. https://doi.org/10.1016/0304-386X(76)90004-9.

[81] X. Yang, M.S. Moats, J.D. Miller, The interaction of thiourea and formamidine disulfide in the dissolution of gold in sulfuric acid solutions, Miner. Eng. 23 (2010) 698–704. https://doi.org/10.1016/j.mineng.2010.04.006.

[82] J.P. Shubha, Puttaswamy, Oxidative conversion of thiourea and N -substituted thioureas into formamidine disulfides with acidified chloramine-T: a kinetic and mechanistic approach, J.

Sulfur Chem. 30 (2009) 490–499. https://doi.org/10.1080/17415990902725725.

[83] M. Yamada, M.R. Gandhi, Y. Kaneta, Y. Hu, A. Shibayama, Calix[4]arene-based n-dialkylamino extractants for selective platinum group metal separation from automotive catalysts, ChemistrySelect 2 (2017) 1052–1057. https://doi.org/10.1002/slct.201601981.

[84] F. Casanova, R. Freixo, C.F. Pereira, A.B. Ribeiro, E.M. Costa, M.E. Pintado, Ó.L. Ramos, Comparative study of green and traditional routes for cellulose extraction from a sugarcane by-product, Polymers (Basel). 15 (2023) 1251. https://doi.org/10.3390/polym15051251.

[85] D. Prat, A. Wells, J. Hayler, H. Sneddon, C.R. McElroy, S. Abou-Shehada, P.J. Dunn, CHEM21 selection guide of classical- and less classical-solvents, Green Chem. 18 (2016) 288–296. https://doi.org/10.1039/C5GC01008J.

Journal Pre-proof

Declaration of interests

☒ The authors declare that they have no known competing financial interests or personal relationships that could have appeared to influence the work reported in this paper.

☐ The authors declare the following financial interests/personal relationships which may be considered as potential competing interests:

Journal Pre-proof

Graphical abstract

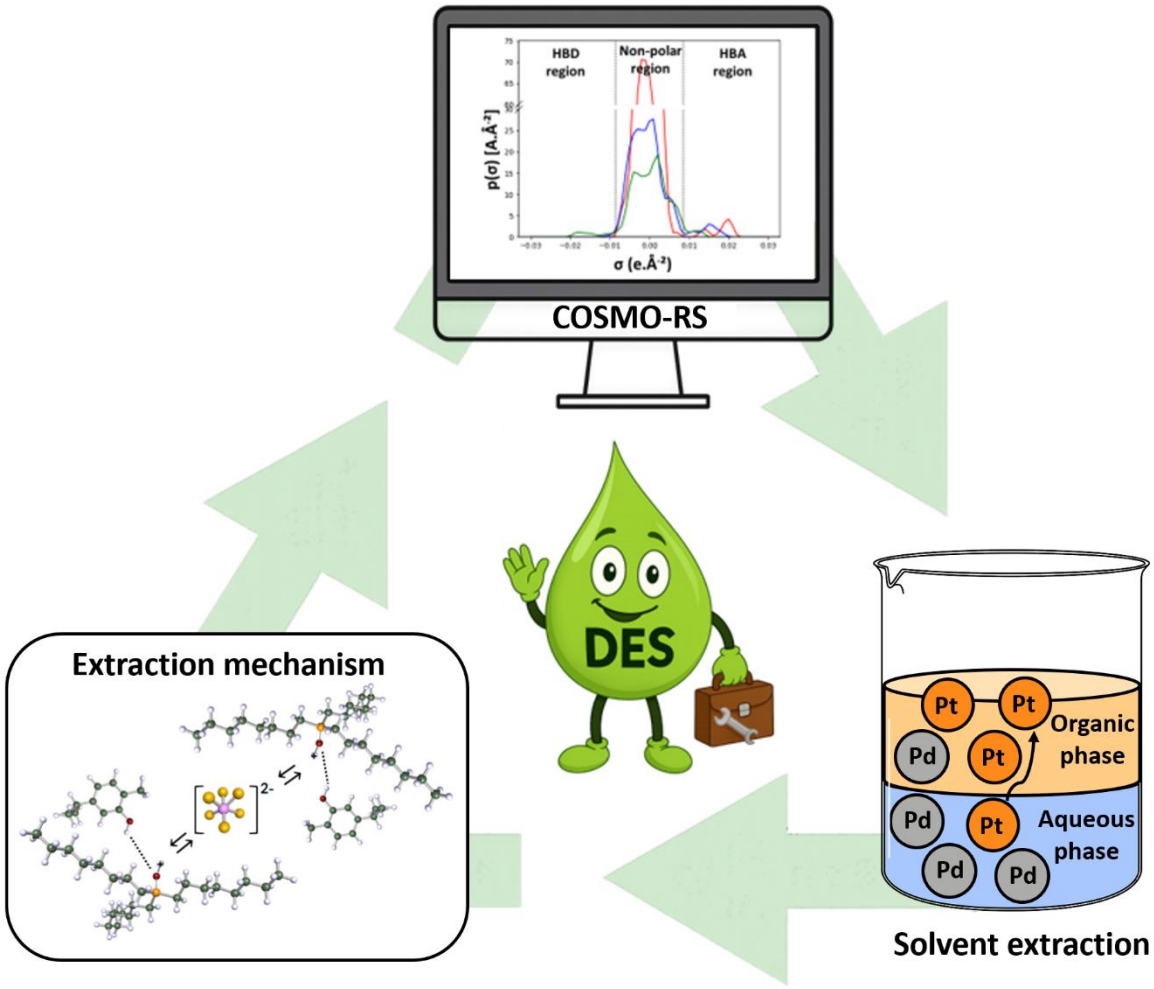

Highlights

- The DESs TOCA and LICA are proposed for selective Pt and Pd extraction
- TOCA and LICA are characterised with thermal, chemical and spectroscopic techniques
- TOCA showed a strong preference for Pt extraction, whereas LICA favoured that of Pd
- The extraction mechanism is based on a neutral ion-pair association
- TOCA shows outstanding recyclability whilst LICA undergoes some leaching

Journal Pre-proof